Free vibration of moderately thick FGM plates using the dynamic stiffness method and the Wittrick-Williams algorithm

Md. Imran Ali[a], M.S. Azam[a], V. Ranjan[b], J.R. Banerjee[c]

[a]Department of Mechanical Engineering, Indian Institute of Technology, Dhanbad 826004, Jharkhand, India
[b]Visiting Professor, Division of Physical and Computational Sciences, University of Pittsburgh Bradford, PA 16701, USA
[c]School of Science and Technology, City St George's, University of London, Northampton Square, London EC1V 0HB, UK

Abstract

The dynamic stiffness method (DSM) for free vibration analysis of functionally graded moderately thick plates based on power and sigmoid laws is developed. The functionally graded plates analysed are identified as P-FG and S-FG plates, describing the power and sigmoid laws. The effective material properties of the P-FG and S-FG plates are assumed to vary through the thickness of the plate. First-order shear deformation theory and Hamilton's principle are used to derive the governing differential equations of motion. The Levy-type solution is sought to derive an efficient analytical formulation for plates with simply supported boundary conditions along two opposite edges. By imposing the boundary conditions for displacements and forces, the dynamic stiffness matrix is developed. Then the Wittrick–Williams (W-W) algorithm is applied to compute the natural frequencies and mode shapes of P-FG and S-FG plates. The influence of the material gradient index, aspect ratio, thickness to length ratio and boundary conditions on the natural frequencies and mode shapes of P-FG and S-FG plates are investigated in detail. Comparing these two grading laws i.e. power and sigmoid grading laws is important, as they yield different stress and stiffness distributions, which directly impact vibration characteristics, stress concentrations, and manufacturability of functionally graded components. To establish the accuracy and validity of results from the present theory, comparative studies utilising existing literature are performed, which show excellent agreement. The results given, can be used as bench-mark solutions when validating finite element and other approximate theories.

Keywords: functionally graded plates, dynamic stiffness method, Wittrick-William algorithm, free vibration analysis, power law, sigmoid law

[*]Corresponding author, e-mail: j.r.banerjee@citystgeorges.ac.uk

1. Introduction

Functionally graded materials (FGMs) have attracted considerable attention in recent years for their large-scale application in various engineering fields such as civil, aerospace, shipbuilding, automobile and nuclear engineering, amongst others. Basically, FGMs are a distinctive class of composite materials for which physical properties are made to change in specified directions based on some designated functions. In general, there are basically two phases of FGMs, namely the metallic and the ceramic and the properties gradually change from one phase to other. Thus, the volume fraction of FGMs varies in direction, generally through the thickness and/or along the length, making one side of the material ceramic while the other side metallic. In this way, the heat-resistant thermal properties of ceramic and the mechanical properties of metal can be exploited to advantage. Thus, FGMs have wide ranging applications in various engineering fields such as aerospace, automobile, ship building, amongst others. The continuous change in the microstructure of FGMs distinguishes them from the conventional fibre-reinforced laminated composite materials, which have understandably a mismatch in mechanical properties across the interface of the two discrete materials, i.e., fibres, and resins that are generally bonded together. As a result, the constituents of the fibre-matrix composites become prone to debonding, particularly under high thermal loading. Furthermore, in fibrous composites cracks are likely to occur at the interfaces between fibre and matrix, which may grow and subsequently reduce the strength and eventually lead to the failure of the structure. Additional problems in fibrous composite materials are associated with the presence of residual stresses that are induced due to the differences in coefficients of thermal expansion of the fibre and the matrix. In FGMs, these problems are circumvented because of the gradual variation in the volume fraction of the constituent material components, rather than an abrupt change of properties across the interface, as prevalent in fibrous composites [1-2]. These beneficial qualities distinguish FGMs from their traditional composite counterparts and thus make them the ideal choice for applications in optoelectronics, biomedical, chemical, mechanical, spacecraft and many other essential engineering requirements [3]. Continuous variations of the volume fraction of two and more materials through the thickness direction of a structure, e.g., a plate or a beam, are generally modelled by some power law, such as sigmoidal and/or exponential law.

Many researchers have utilised power law [4, 5] or exponential law [6–11] through the thickness direction in order to characterise the variation of material properties in FGMs.

However, in both power and exponential laws, the stress concentration in FGMs may occur in one of the interfaces in which the material property variation may be continuous but rapidly changing [12]. Against this background, Chi and Chung [13] proposed a sigmoid FGM, which is composed of two power-law functions to define a new volume fraction. They also indicated that the use of a sigmoid FGM can significantly reduce the stress intensity factors. It should be noted that P-FG distributions are commonly employed due to their mathematical simplicity and widespread acceptance while S-FG distributions offer smoother transitions in material properties, which can help reduce stress concentrations and improve overall structural performance. Additionally, the inclusion of S-FG models allows one to assess the computational implications of using more complex grading profiles.

In the context of the current research, it is well known that the neutral surface (NS) of a plate is characterized by the surface that is free from strain and stress when the plate is subjected to pure bending. For a homogeneous isotropic or for a symmetrically laminated plate, the neutral surface and the geometric middle surface are essentially the same whereas the NS of a functionally graded plate may not coincide with its mid-surface because of the material property variation through the thickness of the plate [14]. In this respect, the concept of NS was highlighted by Zhang and Zhou [15], Yin et al. [16], Kim and Lee [17], Lee et al.[18], and Zhang [19] when deriving the governing equations for a functionally graded (FG) plate. The introduction of NS in the analysis is advantageous because it eliminates the coupling between the membrane and the curvature modes. Such a coupling can give rise to enormous difficulties to formulate the problem.

Free vibration of FGM plates have been studied quite extensively in the literature to understand the response behaviour of plates, e.g., see [3]. From an engineering point of view, the importance of this topic cannot be underestimated or overemphasized, especially for its promising application in aircraft design because the upper and lower surfaces of the wing are typically idealized by plates or plate assemblies. In recent years, extensive efforts have been expended to improve the modeling and analysis of free vibration characteristics of functionally graded (FG) and composite structures. Several researchers have presented novel numerical and analytical methods to capture the vibrational response of FG plates and similar structural elements under various boundary and loading conditions. Benadouda et al. [20] conducted a comprehensive analysis of wave propagation in functionally graded beams with defects, highlighting the effects of porosity and cracks on dynamic responses. Lakel et al. [21] studied the free vibration behavior of functionally graded graphene nanoplatelet-reinforced (FG-

GNPR) nanoplates using a refined plate theory and Eringen's nonlocal elasticity model. Their work investigated the influence of GNP distribution, nonlocal effects, and boundary conditions on natural frequencies, providing valuable insights for nanoscale structural design. Ghalem et al. [22] analyzed the free vibration of 2D-FG beams with internal cracks on Winkler–Pasternak foundations using the h-finite element method, highlighting the effects of crack parameters and material gradation on natural frequencies. Their investigation offered valuable insights into the dynamic behavior of cracked FG structures. On the other hand, Khayra et al. [23] studied the free vibration behavior of cracked functionally graded plates considering porosity defects and various material gradation types, showing that porosity distribution and boundary conditions significantly affect the natural frequencies. Their findings provided important insights into the dynamic response of imperfect FGM structures. The application of FGMs thus plays a significant role to enhance the design of aircraft wings for which the free vibration analysis is a very important consideration, particularly from a dynamic standpoint.

With the emergence of powerful computational processors, the tendency to use Finite Element Method (FEM) for structural analysis has increased immensely. The FEM is after all an approximate numerical method, but the result from FEM generally converges to exact result with increasing number of elements [24]. It is well-recognised that the accuracy of results from FEM cannot be always guaranteed. This is particularly true in dynamic analysis at high frequencies when the FEM may become inaccurate or even unreliable. Nevertheless, the FEM serves as the most convenient computational method to analyse complex structures with complex geometries and boundaries. The FEM being a numerical method, by its very nature, requires considerable computational resources and CPU time, especially when carrying out optimization studies. The computational effort can, of course be minimized if accurate and efficient analytical methods are developed, particularly to validate and enhance the performance of FEM. One such method is the dynamic stiffness method (DSM) [25–31] which gives exact results that are independent of the number of elements used in the analysis, which is in sharp contrast to FEM. For instance, one single structural element can be used in the DSM to compute any number of natural frequencies of a structure to any desired accuracy, which, of course, is impossible in the FEM. In DSM, once the initial assumptions about the displacement field have been made leading to the governing differential equations of motion of a structural element, no additional assumptions are made in the analysis [32]. A literature survey shows that many remarkable contributions in DSM have been made over the years [33-39] in free vibration analysis of isotropic and orthotropic plates. By and large, researchers have utilized the Wittrick-

Williams (W-W) algorithm as solution technique when using the DSM, (see [40-45]) for free vibration analysis of isotropic and anisotropic beams and plates. Pagani et al. [46] developed the DSM for computing the eigenvalue of composite beams under different boundary (edge) conditions whereas Kolarevic et al. [47] employed the superposition and projection method to formulate the DSM for rectangular plate assemblies.

For FG plate problems, two key issues need to be primarily addressed. These are: the modelling of the plate using an appropriate plate theory, and the solution procedure. The first issue which is basically about the choice of plate theories which can be generally classified into three major categories: thin plate theory based on Kirchhoff-Love plate theory (KLPT), moderately thick plate theory based on Reissner–Mindlin plate or first-order shear deformation theory (FSDT), and thick plate theory based on higher order shear deformation theory (HSDT) or third-order shear deformation theory (TSDT). It is well-known that KLPT being a relatively simple plate theory can be applied to thin plates reasonably successfully, but for thick plates, KLPT may give poor results, particularly for higher order natural frequencies and mode shapes because KLPT does not account for the effect of shear deformation which becomes significant through the thickness direction of thick plates. There are many researchers who used KLPT to study the dynamic behaviour of isotropic and FGM plates. For instance, Liessa [48] applied KLPT to investigate the free vibration behaviour of isotropic thin rectangular plates whereas a combination of KLPT and Rayleigh–Ritz method was used by Chakraverty et al. [49] to analyse FGM plates for their free vibration characteristics. On the other hand, Abrate [50] investigated the free vibration behaviour of FGM plates with simply supported and clamped boundary (edge) conditions using KLPT. To overcome the limitations of KLPT, the First-order Shear Deformation Theory (FSDT) which accounts for the effect of shear deformation was formulated by Reissner [51] and Mindlin [52] who introduced the application of a rather fictitious shear correction factor to account for the non-uniform shear stress distribution through the thickness of the plate in an attempt to satisfy the zero-stress condition at the outer surface of the plate, on an ad-hoc basis. The concept of shear correction factor is an approximate idea, and it may not be always satisfactory because a change in the material properties, loading cases and boundary (edge) conditions can cause a change in the value of the shear correction factor, which may affect the accuracy of results. First-order shear deformation theory (FSDT) is appropriate for moderately thick plates because it accounts for transverse shear deformation, rotatory inertia and dispenses with the idea of fictitious shear correction factor while keeping the formulation fairly simple and computationally efficient. It strikes a balance between accuracy and complexity, especially compared to higher-order theories, which may become complex and computationally intensive. However, experience has shown that for moderately thick plates, FSDT is expected to give reasonably good results. Reissner and Mindlin’s original idea [51, 52] of using FSDT was picked up by subsequent researchers who used FSDT to investigate functionally graded plates. Thai et al. [53] presented an FSDT approach to carry out the free vibration analysis of functionally graded plates. By contrast, Meksi et al. [54] developed a new first-order shear deformation (NFSDT) based on NS position for static bending and free vibration analysis of FG plates supported by an elastic foundation. Hosseini-Hashemi et al. [55] used an exact analytical solution to investigate the natural vibration of FGM plates via Reissner–Mindlin plate theory under Levy-type boundary (edge) conditions. They discussed the effects of aspect ratio, thickness-to-length ratio, material gradient index and boundary (edge) conditions on results. Thai and Choi [56] developed a simple first-order shear deformation theory (SFSDT) for the natural vibration analysis of FGM plates under simply supported boundary (edge) condition using closed-form solutions. It should be noted from [56] that unlike conventional FSDT, SFSDT contains only four unknowns and has striking similarities with KLPT in many aspects, for instance, in terms of the governing differential equations, boundary (edge) conditions, etc. On the other hand, Hosseini-Hashemi et al. [57] presented an analytical solution for the natural vibration analysis of elastically supported FGM plates subjected to Levy-type boundary (edge) conditions via FSDT. The gradation of material properties of the FGM plates obeyed the power law function in their work. Free vibration analysis of moderately thick rectangular FGM plates with general elastic boundary (edge) conditions was performed by Li et al. [58] using an accurate solution method based on Reissner–Mindlin plate theory. Bellifa et al. [59] developed a new FSDT for the dynamic and static analyses of FGM plates considering a NS. The equation of motion and boundary condition of the FGM plate were derived by them via FSDT. Fallah et al. [60] implemented the extended Kantorovich method in FSDT to investigate the natural vibration of moderately thick FGM plates supported by elastic supports, but with different combinations of clamped and simply supported boundary (edge) conditions. They discussed the effects of elastic foundation, geometric parameter, boundary (edge) condition on the eigenvalues of the plate. Yin et al. [61] carried out free vibration analysis of FGM plates using the concept of neutral surface (NS) and isogeometric method, which is basically a computational method, integrating the finite element method (FEM) as a tool. They compared their solutions with those obtained by KLPT without introducing the concept of NS. They also compared their results with those obtained from FSDT and exact solutions. Clearly, the introduction of the NS concept helped these investigators to eliminate the coupling of the mid-plane displacement effects on the free vibration analysis. Recent studies have introduced advanced shear deformation theories to investigate the dynamic behavior of porous and bi-directional FGM beams and plates, accounting for effects such as stretching, foundation variability, and thermal loading [62–67]. These works employ quasi-3D, refined, and higher-order shear deformation theories, offering improved accuracy without using shear correction factors. The present study builds upon this foundation to enhance analytical efficiency and reliability in vibration analysis of moderately thick FG plates. There are other contributors who inspired this work, for examples, Bennai et al. [68] developed a refined hyperbolic shear and normal deformation theory to analyze the bending, vibration, and buckling behaviour of functionally graded sandwich beams, accounting for both transverse shear and normal deformations. Their analytical solutions demonstrated the influence of material gradation, boundary conditions, and thickness ratios on the structural responses of FG sandwich beams. Notably Dahmane et al. [69] presented a higher-order shear deformation theory to study the wave propagation in bi-directional porous functionally graded cantilever beams, considering material gradation in both thickness and width directions. Their theory and results, obtained using Hamilton's principle, revealed significant effects of porosity distribution, wave number, and volume fraction indices on the dynamic response, with uneven porosity yielding higher natural frequencies. By contrast, Mellal et al. [70] developed a three-variable higher-order shear deformation theory to investigate the free vibration and buckling behavior of porous functionally graded beams resting on variable elastic foundations, incorporating diverse porosity distributions and foundation stiffness variations, and demonstrated its accuracy and simplicity through analytical solutions and validation with existing literature. Bennai et al. [71] analyzed the buckling and free vibration responses of imperfect porous functionally graded beams using a higher-order shear strain theory, considering both power-law and sigmoid distributions of material properties through the thickness and introducing a novel porosity distribution to evaluate its influence on the mechanical behavior with improved accuracy over earlier models. Kehli et al. [72] developed a four-unknown quasi-3D HSDT for cracked FG beams on viscoelastic foundations, showing accurate vibration analysis without shear correction factors. Hadji et al. [73] investigated the free vibration behavior of functionally graded sandwich rectangular plates using a four-variable refined plate theory (RPT), which eliminates the need for shear correction factors and ensures parabolic distribution of transverse shear stresses, providing accurate and efficient closed-form solutions for various sandwich configurations. Zouatnia and Hadji [74] proposed a simple four-unknown HSDT for analyzing static and vibration responses of FGM sandwich plates without requiring shear correction factors. Sahan [75] proposed an efficient

Laplace-based analytical method using FSDT for transient vibration analysis of doubly-curved laminated shells. The approach was validated against FEM and Newmark solutions, showing high accuracy. Temel and Noori [76] developed a unified numerical method using FSDT and Laplace transform to analyze 2D-FG circular and annular plates with variable thickness, showing excellent accuracy against FEM results. Zairi et al. [77] developed a hybrid finite element model based on Sanders' shell theory to study the free vibration and aeroelastic instability of FG plates, showing excellent accuracy under various boundary conditions. Temel and Sahan [78] developed a finite element method combined with Laplace transform techniques to analyze the damped dynamic response of laminated Mindlin plates, effectively accommodating both elastic and viscoelastic materials. On the other hand, Dhuria et al. [79] proposed a secant hyperbolic higher-order shear deformation theory to study the bending and buckling behavior of porous P-FGM and S-FGM plates using a refined finite element approach.

To the best of the authors' knowledge, the DSM has not yet been applied to investigate the natural vibration characteristics of moderately thick P-FG and S-FG plates based on power law controlled and sigmoid law controlled functionally graded materials. Therefore, the authors of this paper have endeavoured to use the DSM in conjunction with the W-W algorithm to study the free vibration characteristics of the moderately thick P-FG and S-FG rectangular plates. It will be shown later that the results of their investigation are very accurate when compared to those available in the literature. In the analysis put forward the kinematic variables of the plate are described using the FSDT. To verify the predictable accuracy of results from the proposed theory for free vibration of FGM plates using DSM and the W-W algorithm, a wide range of numerical results are presented and a substantial amount of them are validated. The results from the current analysis may serve as benchmark solutions for those researchers who wish to validate their own theories and results.

2. Methodology

2.1. Mathematical modelling

A schematic representation of a plate in a rectangular Cartesian coordinate system (x, y, z) is shown in Fig.1. The upper part of the plate is made of pure ceramic while the bottom part consists of pure metal. The continuous variation of the volume fraction of two materials (ceramic and metal) along the thickness direction of the plate is modelled according to power law and sigmoidal law functions, as follows.

The power law function of P-FG plate is defined as [80].

$$P(z_{ms}) = P_u V_c + P_l\ (1 - V_c) \tag{1}$$

where $P(z_{ms})$ represents typical properties somewhere in the middle, and P_u and P_l are the properties of the upper (ceramic) and lower (metal) surfaces of the plate, respectively, and V_c is the volume fraction of the ceramic, defined as:

$$V_c = \left(0.5 + \frac{z_{ms}}{h}\right)^k \tag{2}$$

where k (Note that k >0) represents the material gradient index which controls the volume fraction of the material in the transverse direction.

With the help of equations (1) and (2), elastic modulus $E(z_{ms})$ and density $\rho(z_{ms})$can be defined as [80].

$$\left.\begin{aligned} E(z_{ms}) &= E_m(z_{ms}) + (0.5 + \frac{z_{ms}}{h})^k [E_c(z_{ms}) - E_m(z_{ms})] \\ \\ \rho(z_{ms}) &= \rho_m(z_{ms}) + (0.5 + \frac{z_{ms}}{h})^k [\rho_c(z_{ms}) - \rho_m(z_{ms}) \end{aligned}\right\} \tag{3}$$

where the subscripts c and m correspond to ceramic and metal, respectively.

The variation of volume fractions $V_f(z_{ms})$ of the constituents of the S-FG plate through the thickness direction when given by sigmoid law functions is as follows [12].

$$\left.\begin{aligned} V_f{}^1(z_{ms}) &= \frac{1}{2}\left(\frac{h/2 + z_{ms}}{h/2}\right)^k & -h/2 \le z_{ms} \le 0 \\ V_f{}^2(z_{ms}) &= 1 - \frac{1}{2}\left(\frac{h/2 - z_{ms}}{h/2}\right)^k & 0 \le z_{ms} \le h/2 \end{aligned}\right\} \tag{4}$$

where, k represents the non-negative sigmoid volume fraction index (material gradient index) that controls the volume fraction of the material through the thickness direction.

The sigmoid law function of S -FG plate is defined as [12].

$$\left.\begin{aligned} P_1(z_{ms}) &= V_f{}^1(z_{ms})P_c + [1 - V_f{}^1(z_{ms})]P_m & -h/2 \le z_{ms} \le 0 \\ P_2(z_{ms}) &= V_f{}^2(z_{ms})P_c + [1 - V_f{}^2(z_{ms})]P_m & 0 \le z_{ms} \le h/2 \end{aligned}\right\} \tag{5}$$

where $P_1(z_{ms})$ and $P_2(z_{ms})$ represent the typical material properties such as Young's modulus (E), material density(ρ) and Poisson's ratio (ν). In equation (5), P_c and P_m are the material properties of the ceramic and metal, respectively.

Figure 1 also shows the position of neutral surface and middle surface for an FGM plate which are separated by a distance 'a'. The concept of neutral surface was elaborated by Ali et al. [12] and therefore, no detailed elucidation is needed. As the neutral surface takes a new coordinate system, where its position can be defined as follows:

$$z_{ms} - z_{ns} = a \tag{6}$$

2.2 First-order shear deformation theory (FSDT)

This section represents the formulation of the natural vibration behavior of moderately thick P-FG and S-FG plates by using FSDT.

The displacement field for the P-FG or S-FG plate based on neutral surface is given by [12, 80, 81].

$$\left.\begin{aligned} u(x,y,z,t) &= u_0(x,y,t) - z_{ns}\varphi_y(x,y,t) \\ v(x,y,z,t) &= v_0(x,y,t) - z_s\varphi_x(x,y,t) \\ w(x,y,z,t) &= w_0(x,y,t) \end{aligned}\right\} \tag{7}$$

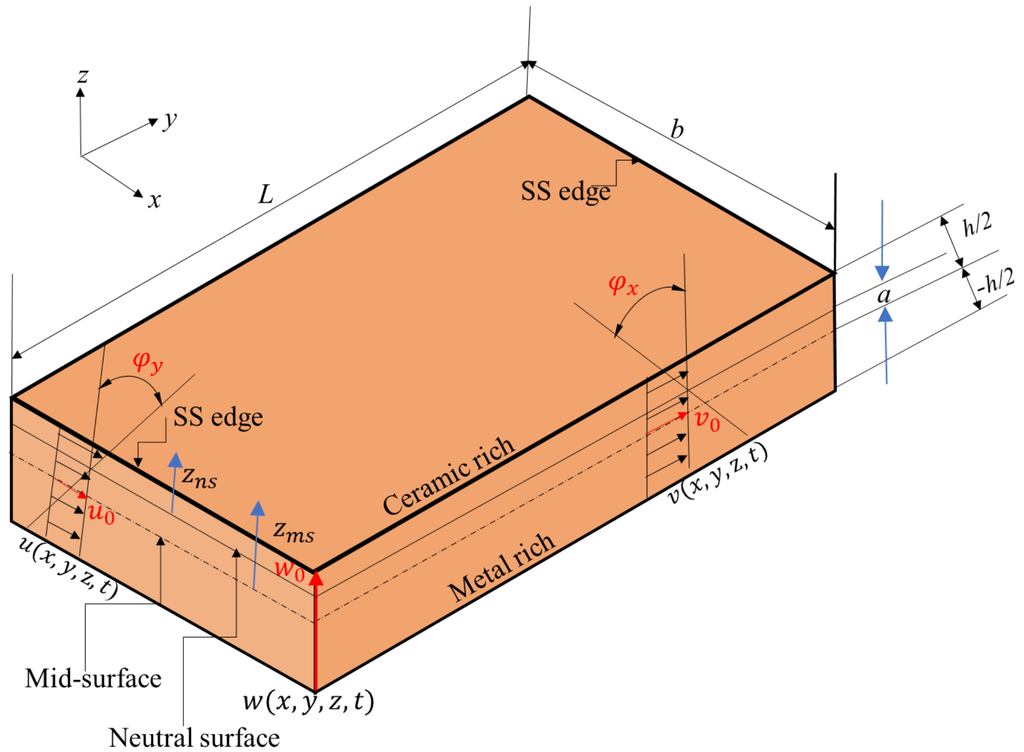

Fig.1. Coordinate system and notations for a FGM plate

where u_0 and v_0 are the inplane (membrane) displacements and w_0 is the transverse displacement of a point on the mid-plane, φ_x and φ_y are the bending rotations about the x and y axes, respectively.

The displacement field is carefully chosen to work out the kinetic and potential energies which will lead to the governing differential equations of motion of the FGM plate when applying Hamilton's principle. In this way, the three coupled governing partial differential equations were derived, and they are given by [32].

$$\left.\begin{aligned}
&K_s G h\left(\frac{\partial^2 w^0}{\partial x^2}+\frac{\partial \varphi_y}{\partial x}-\frac{\partial \varphi_x}{\partial y}+\frac{\partial^2 w^0}{\partial y^2}\right)-\rho(z_{ns})h\frac{\partial^2 w^0}{\partial t}=0\\
&D^*\left(\frac{\partial^2 \varphi_y}{\partial x^2}+\left(\frac{1-\nu}{2}\right)\frac{\partial^2 \varphi_y}{\partial y^2}-\left(\frac{1+\nu}{2}\right)\frac{\partial^2 \varphi_x}{\partial y \partial x}\right)-K_s G h\left(\frac{\partial w^0}{\partial x}+\varphi_y\right)-\frac{\rho(z_{ns})h^3}{12}\frac{\partial^2 \varphi_y}{\partial t^2}=0\\
&D^*\left(\frac{\partial^2 \varphi_x}{\partial y^2}+\left(\frac{1-\nu}{2}\right)\frac{\partial^2 \varphi_x}{\partial x^2}-\left(\frac{1+\nu}{2}\right)\frac{\partial^2 \varphi_y}{\partial y \partial x}\right)+K_s G h\left(\frac{\partial w^0}{\partial y}-\varphi_x\right)-\frac{\rho(z_{ns})h^3}{12}\frac{\partial^2 \varphi_x}{\partial t^2}=0
\end{aligned}\right\}\quad(8)$$

where $G=\frac{E(z_{ns})}{2(1+\text{v})}$ is the modulus of rigidity or shear modulus, K_s is the shear correction factor taken to be 5/6 in accordance with Reissner [51] and $D^*=\int_{\frac{-h}{2}-a}^{\frac{h}{2}-a}E(z_{ns})z_{ns}{}^2dz_{ns}/(1-\text{v}^2)$ which is alternatively given by $D^*=\frac{\int_{-h/2-a}^{0}z_{ns}^2\,E(z_{ns})dz_{ns}}{1-\text{v}^2}+\frac{\int_{0}^{h/2-a}z_{ns}^2\,E(z_{ns})dz_{ns}}{1-\nu^2}$ is the flexural rigidity of the P-FG and S-FG plate for which the Young's modulus $E(z_{ns})$ vary in accordance with the power law and sigmoid law functions of the FGM plate and ν is the Poisson's ratio, which is assumed to be constant.

The natural boundary conditions (BCs) resulting from the Hamiltonian formulation, lead to the expressions for shear force (Q_x), bending moment (M_{xx}) and twisting moment (M_{xy}) as follows [32].

$$\left.\begin{aligned}
&Q_x : K_s G h\left(\frac{\partial w^0}{\partial x}+\varphi_y\right)\delta w^0,\\
&M_{xx} : D^*\left(\frac{\partial \varphi_y}{\partial x}-\nu\frac{\partial \varphi_x}{\partial y}\right)\delta\varphi_y,\\
&M_{xy} : -\frac{Gh^3}{12}\left(\frac{\partial \varphi_y}{\partial y}-\frac{\partial \varphi_x}{\partial x}\right)\delta\varphi_x.
\end{aligned}\right\}\quad(9)$$

Note that the dynamic stiffness matrix developed for the FGM plates is based on the Levy type solutions of the governing differential equations so that the two opposite sides (parallel to *x*-

axis in Fig. 1) are simply supported. Therefore, the expression for the bending moment M_{yy} is not so relevant in this case and hence not shown in Eq. (9). Equations (8) and (9) are the basic requirements to develop the DS matrix of the FGM plates using FSDT.

2.3 Formulation of the dynamic stiffness matrix for the FGM plate via FSDT

The solution of Eq. (8) is sought in the traditional Levy form (two opposite edges of the plate are simply supported at y=0 and y=L). Solutions that meet these conditions can be expressed as follows [32].

$$\left.\begin{aligned} w^0(x,y,t) &= \sum_{\mathrm{m}=1}^{\infty} W_m(x)e^{i\omega t}\sin(\alpha_m y) \\ \varphi_y(x,y,t) &= \sum_{\mathrm{m}=1}^{\infty} \varphi_{y_m}(x)e^{i\omega t}\sin(\alpha_m y) \\ \varphi_x(x,y,t) &= \sum_{\mathrm{m}=1}^{\infty} \varphi_{x_m}(x)e^{i\omega t}\cos(\alpha_m y) \end{aligned}\right\} \quad (10)$$

where ω is the circular or angular frequency and $\alpha_m = \frac{m\pi}{L}$ $(m = 1,2 \ldots\ldots\ldots\ldots\ldots \infty)$, and L is the length of the plate.

Substituting Eq. (10) into Eq. (8), the following ordinary differential equation of motion is obtained:

$$\left.\begin{aligned} & GhK_s\frac{\mathrm{d}^2W_m}{\mathrm{d}x^2} + (h\omega^2\rho(z_{ns}) - \alpha^2 GhK_s)W_m + \alpha GhK_s\varphi_{x_m} + GhK_s\frac{\mathrm{d}\varphi_{y_m}}{\mathrm{d}x} = 0 \\ & D^*\frac{\mathrm{d}^2\varphi_{y_m}}{\mathrm{d}x^2} - GhK_s\frac{\mathrm{d}W_m}{\mathrm{d}x} + \alpha D^*\frac{1+\nu}{2}\frac{\mathrm{d}\varphi_{x_m}}{\mathrm{d}x} + \left(\alpha^2 D^*\frac{\nu-1}{2} - GhK_s + \frac{\omega^2\rho(z_{ns})h^3}{12}\right)\varphi_{y_m} = 0 \\ & D^*\frac{1-\nu}{2}\frac{\mathrm{d}^2\varphi_{x_m}}{\mathrm{d}x^2} + \alpha GhK_s W_m - \alpha D^*\frac{1+\nu}{2}\frac{\mathrm{d}\varphi_{y_m}}{\mathrm{d}x} + \left(\frac{\omega^2\rho(z_{ns})h^3}{12} - \alpha^2 D^* GhK_s\right)\varphi_{x_m} = 0 \end{aligned}\right\} (11)$$

Equation (11) can be expressed in the following matrix form.

$$\begin{bmatrix} H & GhK_sX & \alpha GhK_s \\ -GhK_sX & I & \alpha D^*\dfrac{1+\nu}{2}X \\ \alpha GhK_s & \alpha D^*\dfrac{1+\nu}{2}X & J \end{bmatrix}\begin{bmatrix} W_m \\ \varphi_{y_m} \\ \varphi_{x_m} \end{bmatrix} = \begin{bmatrix} 0 \\ 0 \\ 0 \end{bmatrix} \quad (12)$$

where

$$\left.\begin{aligned} H &= h\omega^2\rho(z_{ns}) + GhK_s(X^2 - \alpha^2) \\ I &= D^*\left(X^2 + \alpha^2\frac{\nu-1}{2}\right) - GhK_s + \frac{\omega^2\rho(z_{ns})h^3}{12} \\ J &= D^*\left(\frac{1-\nu}{2}X^2 - \alpha\right) + \frac{\omega^2\rho(z_{ns})h^3}{12} - GhK_s \end{aligned}\right\} (13)$$

with X being the differential operator $\frac{\mathrm{d}}{\mathrm{d}x}$.

The 3×3 determinant of Eq. (12) is expanded so that the following GDE, satisfying all the three displacement variables W_m , φ_{y_m} and φ_{x_m}, each denoted by Ψ is obtained.

$$(X^6 + a_1 X^4 + a_2 X^2 + a_3 X)\Psi = 0 \tag{14}$$

where

$$\left.\begin{aligned}
a_1 &= \frac{\left\{24G^2hK_s{}^2 + Gh^3K_s\omega^2\rho(z_{ns})(\nu-3) - (36\alpha^2D^*GK_s - 12D^*\omega^2\rho(z_{ns}))(\nu-1)\right\}}{12D^*GK_s(\nu-1)} \\
a_2 &= \frac{\left\{\begin{matrix} \left(h\omega^2\rho(z_{ns})(12GK_s - h^2\omega^2\rho(z_{ns}))(Gh^3K_s - 6D^*(\nu-3)\right) \\ -12\alpha^2D^*\left(24G^2hK_s{}^2 + Gh^3K_s\omega^2\rho(z_{ns})(\nu-3) + 12D^*\omega^2\rho(z_{ns})(\nu-1)\right) \\ +216\alpha^4D^{*2}GK_s(\nu-1) \end{matrix}\right\}}{72D^{*2}GK_s(\nu-1)} \\
a_3 &= \frac{\left\{\begin{matrix} -\left((12\alpha^4D^*GK_s - (12GhK_s + \alpha^2(12D^* + Gh^3K_s))\omega^2\rho(z_{ns}) + h^3\omega^4\rho(z_{ns})^2)\right) \\ -(12GhK_s + h^3\omega^2\rho(z_{ns}) + 6\alpha^2D^*(\nu-1)) \end{matrix}\right\}}{\left(72D^{*2}GK_s(\nu-1)\right)}
\end{aligned}\right\} \tag{16}$$

Substituting a trial solution e^{λ} in Eq. (14) gives the following auxiliary equation.

$$(\lambda^6 + a_1\lambda^4 + a_2\lambda^2 + a_3) = 0 \tag{15}$$

The 6th order polynomial equation of Eq. (15) can be reduced to a cubic by replacing λ^2 by μ to give

$$(\mu^3 + a_1\mu^2 + a_2\mu + a_3) = 0 \tag{17}$$

The roots of Eq. (17) are then calculated as follows:

$$\left.\begin{aligned}
\mu_1 &= -\frac{1}{3}\left(a_1 + \sqrt[3]{\frac{p+\sqrt{q}}{2}} + \sqrt[3]{\frac{p-\sqrt{q}}{2}}\right), \\
\mu_2 &= -\frac{1}{3}\left(a_1 + \beta_2\sqrt[3]{\frac{p+\sqrt{q}}{2}} + \beta_1\sqrt[3]{\frac{p-\sqrt{q}}{2}}\right), \\
\mu_3 &= -\frac{1}{3}\left(a_1 + \beta_1\sqrt[3]{\frac{p+\sqrt{q}}{2}} + \beta_2\sqrt[3]{\frac{p-\sqrt{q}}{2}}\right),
\end{aligned}\right\} \tag{18}$$

where

$$\begin{gathered}
\beta_1 = \frac{i\sqrt{3}-1}{2}, \qquad \beta_2 = -\frac{i\sqrt{3}+1}{2} \\
p = 2a_1{}^3 - 9a_1a_2 + 27a_{3,} \qquad l = a_1{}^2 - 3a_2, \quad q = p^2 - 4l^3
\end{gathered} \tag{19}$$

The discriminant of the Eq. (17) can be expressed as:

$$\Delta = 18\, a_1 a_2 a_3 - 4{a_1}^3 a_3 + {a_1}^2 {a_2}^2 - 4{a_2}^2 - 27{a_3}^2 \\ = \frac{1}{746496 {D^*}^6 G^4 {K_s}^4 (v-1)^4} \Big(h^2\omega^2\rho(z_{ns})(h^2\omega^2\rho(z_{ns}) - 12GK_s)^2 \big(576D^* G^2 h{K_s}^2 + \\ (gh^3K_s - 12D^*)^2\omega^2\rho(z_{ns})\big)\big(Gh^3K_s\omega^2\rho(z_{ns})(1+\nu) + 6D^*\omega^2\rho(z_{ns})(\nu^2-1) - \\ 24G^2h{K_s}^2\big)^2\Big) \tag{20}$$

Since, discriminant, $\Delta > 0$ which implies that the three roots are real, and therefore there are only four possible solutions which are as follows:

i. All roots are positive.

ii. One positive and two negative roots.

iii. Two positive and one negative roots.

iv. All roots are negative.

Case 1: all roots are positive i.e. μ_1, μ_2 , $\mu_3 > 0$.

Thus for Case 1, all six roots λ of Eq. (15) will be real which are, say, Υ_1, $-\Upsilon_1$, Υ_2 , $-\Upsilon_2$, Υ_3 , $-\Upsilon_3$ where $\Upsilon_1 = \sqrt{\mu_1}$, $\Upsilon_2 = \sqrt{\mu_2}$ and $\Upsilon_3 = \sqrt{\mu_3}$.

Accordingly, the solution of Eq. (14) can be expressed as:

$$\left.\begin{aligned} W_m(x) &= A_{1_m}\cosh(\Upsilon_{1_m}x) + A_{2_m}\sinh(\Upsilon_{1_m}x) + A_{3_m}\cosh(\Upsilon_{2_m}x) + \\ &\quad A_{4_m}\sinh(\Upsilon_{2_m}x) + A_{5_m}\cosh(\Upsilon_{3_m}x) + A_{6_m}\sinh(\Upsilon_{3_m}x) \\ \varphi_{y_m}(x) &= B_{1_m}\cosh(\Upsilon_{1_m}x) + B_{2_m}\sinh(\Upsilon_{1_m}x) + B_{3_m}\cosh(\Upsilon_{2_m}x) + \\ &\quad B_{4_m}\sinh(\Upsilon_{2_m}x) + B_{5_m}\cosh(\Upsilon_{3_m}x) + B_{6_m}\sinh(\Upsilon_{3_m}x) \\ \varphi_{x_m}(x) &= C_{1_m}\cosh(\Upsilon_{1_m}x) + C_{2_m}\sinh(\Upsilon_{1_m}x) + C_{3_m}\cosh(\Upsilon_{2_m}x) + \\ &\quad C_{4_m}\sinh(\Upsilon_{2_m}x) + C_{5_m}\cosh(\Upsilon_{3_m}x) + C_{6_m}\sinh(\Upsilon_{3_m}x) \end{aligned}\right\} \tag{21}$$

Case 2: Two positive roots and one negative root i.e. μ_1 ,μ_2>0 and μ_3<0.

The roots in this case are Υ_1,-Υ_1 ,Υ_2 ,-Υ_2 ,$i\Upsilon_3$,-$i\Upsilon_3$ where $\Upsilon_1 = \sqrt{\mu_1}$, $\Upsilon_2 = \sqrt{\mu_2}$ and $\Upsilon_3 = \sqrt{-\mu_3}$.

Accordingly, the solution of Eq. (14) can be expressed as:

$$\left.\begin{array}{c}W_m(x) = A_{1_m}\cosh(\Upsilon_{1_m}x) + A_{2_m}\sinh(\Upsilon_{1_m}x) + A_{3_m}\cosh(\Upsilon_{2_m}x) + \\ A_{4_m}\sinh(\Upsilon_{2_m}x) + A_{5_m}\cos(\Upsilon_{3_m}x) + A_{6_m}\sin(\Upsilon_{3_m}x) \\ \varphi_{y_m}(x) = B_{1_m}\cosh(\Upsilon_{1_m}x) + B_{2_m}\sinh(\Upsilon_{1_m}x) + B_{3_m}\cosh(\Upsilon_{2_m}x) + \\ B_{4_m}\sinh(\Upsilon_{2_m}x) + B_{5_m}\cos(\Upsilon_{3_m}x) + B_{6_m}\sin(\Upsilon_{3_m}x) \\ \varphi_{x_m}(x) = C_{1_m}\cosh(\Upsilon_{1_m}x) + C_{2_m}\sinh(\Upsilon_{1_m}x) + C_{3_m}\cosh(\Upsilon_{2_m}x) + \\ C_{4_m}\sinh(\Upsilon_{2_m}x) + C_{5_m}\cos(\Upsilon_{3_m}x) + C_{6_m}\sin(\Upsilon_{3_m}x)\end{array}\right\} \quad (22)$$

Case 3: One positive root and two negative roots i.e. $\mu_1>0$ and $\mu_2, \mu_3<0$.

In this case, the roots are Υ_1 , -Υ_1 , $i\Upsilon_2$, -$i\Upsilon_2$,$i\Upsilon_3$,-$i\Upsilon_3$ where $\Upsilon_1 = \sqrt{\mu_1}$, $\Upsilon_2 = \sqrt{-\mu_2}$ and $\Upsilon_3 = \sqrt{-\mu_3}$.

Accordingly, solution can be expressed as:

$$\left.\begin{array}{c}W_m(x) = A_{1_m}\cosh(\Upsilon_{1_m}x) + A_{2_m}\sinh(\Upsilon_{1_m}x) + A_{3_m}\cos(\Upsilon_{2_m}x) + \\ A_{4_m}\sin(\Upsilon_{2_m}x) + A_{5_m}\cos(\Upsilon_{3_m}x) + A_{6_m}\sin(\Upsilon_{3_m}x) \\ \varphi_{y_m}(x) = B_{1_m}\cosh(\Upsilon_{1_m}x) + B_{2_m}\sinh(\Upsilon_{1_m}x) + B_{3_m}\cos(\Upsilon_{2_m}x) + \\ B_{4_m}\sin(\Upsilon_{2_m}x) + B_{5_m}\cos(\Upsilon_{3_m}x) + B_{6_m}\sin(\Upsilon_{3_m}x) \\ \varphi_{x_m}(x) = C_{1_m}\cosh(\Upsilon_{1_m}x) + C_{2_m}\sinh(\Upsilon_{1_m}x) + C_{3_m}\cos(\Upsilon_{2_m}x) + \\ C_{4_m}\sin(\Upsilon_{2_m}x) + C_{5_m}\cos(\Upsilon_{3_m}x) + C_{6_m}\sin(\Upsilon_{3_m}x)\end{array}\right\} \quad (23)$$

Case 4: All three roots are negative i.e. $\mu_1, \mu_2, \mu_3<0$. Thus, the roots of Eq. (15) are all imaginary, i.e., $i\Upsilon_1$,$-i\Upsilon_1$, $i\,\Upsilon_2$, $-i\Upsilon_2$, $i\Upsilon_3$, $-i\Upsilon_3$ where $\Upsilon_1 = \sqrt{-\mu_1}$, $\Upsilon_2 = \sqrt{-\mu_2}$ and $\Upsilon_3 = \sqrt{-\mu_3}$.

Accordingly, solution can be expressed as:

$$\left.\begin{array}{c}W_m(x) = A_{1_m}\cos(\Upsilon_{1_m}x) + A_{2_m}\sin(\Upsilon_{1_m}x) + A_{3_m}\cos(\Upsilon_{2_m}x) + \\ A_{4_m}\sin(\Upsilon_{2_m}x) + A_{5_m}\cos(\Upsilon_{3_m}x) + A_{6_m}\sin(\Upsilon_{3_m}x) \\ \varphi_{y_m}(x) = B_{1_m}\cos(\Upsilon_{1_m}x) + B_{2_m}\sin(\Upsilon_{1_m}x) + B_{3_m}\cos(\Upsilon_{2_m}x) + \\ B_{4_m}\sin(\Upsilon_{2_m}x) + B_{5_m}\cos(\Upsilon_{3_m}x) + B_{6_m}\sin(\Upsilon_{3_m}x) \\ \varphi_{x_m}(x) = C_{1_m}\cos(\Upsilon_{1_m}x) + C_{2_m}\sin(\Upsilon_{1_m}x) + C_{3_m}\cos(\Upsilon_{2_m}x) + \\ C_{4_m}\sin(\Upsilon_{2_m}x) + C_{5_m}\cos(\Upsilon_{3_m}x) + C_{6_m}\sin(\Upsilon_{3_m}x)\end{array}\right\} \quad (24)$$

The formulation procedure of DSM for Case 1 is shown below. However, for the rest of the cases, the procedure will be similar, and it is not repeated here for the sake of brevity.

Referring to Case 1, the substitution of Eq. (21) into the governing differential equation (Eq.11), gives the following relationship which relates the constants:

$$
\left.
\begin{array}{llll}
A_{1_m} = -\,\delta_1 B_{2_m}\,, & C_{1_m} & = & -\,\gamma_1 B_{2_m} \\
A_{2_m} = -\,\delta_1 B_{1_m}\,, & C_{2_m} & = & -\,\gamma_1 B_{1_m} \\
A_{3_m} = -\,\delta_2 B_{4_m}\,, & C_{3_m} & = & -\,\gamma_2 B_{4_m} \\
A_{4_m} = -\,\delta_2 B_{3_m}\,, & C_{4_m} & = & -\,\gamma_2 B_{3_m} \\
A_{5_m} = -\,\delta_3 B_{6_m}\,, & C_{5_m} & = & -\,\gamma_3 B_{6_m} \\
A_{6_m} = -\,\delta_3 B_{5_m}\,, & C_{6_m} & = & -\,\gamma_3 B_{5_m}
\end{array}
\right\} \quad (25)
$$

where

$$
\delta_i = \frac{GK_s\left(12GhK_s - h^3\rho(z_{ns})\omega^2 - 6D^*(-1+v)(\alpha^2 - r_i^2)\right)}{6r_i\left(2G^2hK_s{}^2 - D^*GK_s\alpha^2(1+v) + D^*(1+v)\rho(z_{ns})\omega^2 + D^*GK_s(1+v)r_i^2\right)}\,, \quad (26)
$$

$$
\gamma_i = \frac{(12D^*r_i^2 - 12GhK_s + 6D^*\alpha^2(v-1) + h^3\rho(z_{ns})\omega^2)(GK_s(\alpha^2 - r_i^2) - \rho(z_{ns})\omega^2) - 12G^2hK_s{}^2r_i^2}{6\alpha r_i\left(-2G^2hK_s{}^2 + D^*(1+v)(-\rho(z_{ns})\omega^2 + GK_s(\alpha^2 - r_i^2))\right)} \quad (27)
$$

with i=1, 2, 3.

Thus Eq. (21) results in the following expressions in terms of one set of constants B_{1m} to B_{6m}

$$
\left.
\begin{array}{l}
W_m(x) = -(B_{2m}\delta_1\cosh(\Upsilon_{1m}x) + B_{1m}\delta_1\sinh(\Upsilon_{1m}x) + B_{4m}\,\delta_2\cosh(\Upsilon_{2m}x) \\
\qquad + B_{3m}\,\delta_2\sinh(\Upsilon_{2m}x) + B_{6m}\,\delta_3\cosh(\Upsilon_{3m}x) + B_{5m}\,\delta_3\sinh(\Upsilon_{3m}x)) \\
\varphi_{ym}(x) = B_{1m}\cosh(\Upsilon_{1m}x) + B_{2m}\sinh(\Upsilon_{1m}x) + B_{3m}\cosh(\Upsilon_{2m}x) + \\
\qquad B_{4m}\sinh(\Upsilon_{2m}x) + B_{5m}\cosh(\Upsilon_{3m}x) + B_{6m}\sinh(\Upsilon_{3m}x) \\
\varphi_{xm}(x) = -(B_{2m}\,\gamma_1\cosh(\Upsilon_{1m}x) + B_{1m}\gamma_1\sinh(\Upsilon_{1m}x) + B_{4m}\gamma_2\cosh(\Upsilon_{2m}x) \\
\qquad + B_{3m}\gamma_2\sinh(\Upsilon_{2m}x) + B_{6m}\gamma_3\cosh(\Upsilon_{3m}x) + B_{5m}\gamma_3\sinh(\Upsilon_{3m}x))
\end{array}
\right\} \quad (28)
$$

The expressions of forces and moments are obtained by substituting Eq. (28) into Eq. (9)

$$
\begin{aligned}
Q_{xm}(x,y) &= Q_{\mathrm{x_m}}(x)\sin(\alpha_m y) \\
&= -GhK_s(B_{1m}(1 - \delta_1\Upsilon_{1m})\cosh(\Upsilon_{1x}) + B_{2m}(1 - \delta_1\Upsilon_{1m})\sinh(\Upsilon_{1x}) \\
&\quad + B_{3m}(1 - \delta_2\Upsilon_{2m})\cosh(\Upsilon_{2x}) + B_{4m}(1 - \delta_2\Upsilon_{2m})\sinh(\Upsilon_{2x}) \\
&\quad + B_{5m}(1 - \delta_3\Upsilon_{3m})\cosh(\Upsilon_{3x}) + B_{6m}(1 - \delta_3\Upsilon_{3m})\sinh(\Upsilon_{3x}))\sin(\alpha_m y) \qquad (29)
\end{aligned}
$$

$$
\begin{aligned}
M_{xxm}(x,y) = \mathcal{M}_{xx_m}(x)\sin(\alpha_m y) = D^*(&B_{2m}(\Upsilon_{1m} - \alpha\nu\gamma_1)\cosh(\Upsilon_{1m}x) \\
&+ (B_{1m}(\Upsilon_{1m} - \alpha\nu\gamma_1)\sinh(\Upsilon_{1m}x)) \\
&+ (B_{4m}(\Upsilon_{2m} - \alpha\nu\gamma_2)\cosh(\Upsilon_{2m}x)) + (B_{3m}(\Upsilon_{2m} - \alpha\nu\gamma_2)\sinh(\Upsilon_{2m}x)) \\
&+ (B_{6m}(\Upsilon_{3m} - \alpha\nu\gamma_3)\cosh(\Upsilon_{3m}x)) \\
&+ (B_{5m}(\Upsilon_{3m} - \alpha\nu\gamma_3)\sinh(\Upsilon_{3m}x)))\sin(\alpha_m y)
\end{aligned}
\tag{30}
$$

$$
\begin{aligned}
M_{xym}(x,y) = \mathcal{M}_{xy_m}(x)\cos(\alpha_m y) & \\
&= \frac{-1}{12}Gh^3(B_{1m}(\alpha + \gamma_1\Upsilon_{1m})\cosh(\Upsilon_{1m}x) \\
&+ B_{2m}(\alpha + \gamma_1\Upsilon_{1m})\sinh(\Upsilon_{1m}x) + B_{3m}(\alpha + \gamma_2\Upsilon_{2m})\cosh(\Upsilon_{2m}x) \\
&+ B_{4m}(\alpha + \gamma_2\Upsilon_{2m})\sinh(\Upsilon_{2m}x) + B_{5m}(\alpha + \gamma_3\Upsilon_{3m})\cosh(\Upsilon_{3m}x) \\
&+ B_{6m}(\alpha + \gamma_3\Upsilon_{3m})\sinh(\Upsilon_{3m}x))\, cos(\alpha_m y)
\end{aligned}
\tag{31}
$$

The boundary (edge) conditions (see Fig. 2) for displacements and rotations are as follows:

$$
\begin{aligned}
&\text{At} \quad x = 0: \; W_m = W_1, \; \varphi_{y_m} = \varphi_{y_1}, \qquad \varphi_{x_m} = \varphi_{x_1} \\
&\text{At} \quad x = b: \; W_m = W_2, \; \varphi_{y_m} = \varphi_{y_2}, \qquad \varphi_{x_m} = \varphi_{x_2}
\end{aligned}
\tag{32}
$$

Similarly, the boundary (edge) conditions for forces and moments are as follows:

$$
\begin{aligned}
&\text{At} \quad x = 0: \quad \mathcal{Q}_{x_m} = -\mathcal{Q}_1, \qquad \mathcal{M}_{xx_m} = -\mathcal{M}_{xx_1}, \qquad \mathcal{M}_{xy_m} = -\mathcal{M}_{xy_1}, \\
&\text{At} \quad x = b: \quad \mathcal{Q}_{x_m} = \mathcal{Q}_2, \qquad \mathcal{M}_{xx_m} = \mathcal{M}_{xx_2}, \qquad \mathcal{M}_{xy_m} = \mathcal{M}_{xy_2}
\end{aligned}
\tag{33}
$$

By substituting the boundary (edge) conditions of Eq. (32) for displacements and rotations into Eq. (28), gives the following matrix.

$$
\begin{bmatrix} W_1 \\ \varphi_{y_1} \\ \varphi_{x_1} \\ W_2 \\ \varphi_{y_2} \\ \varphi_{x_2} \end{bmatrix}
=
\begin{bmatrix}
0 & -\delta_1 & 0 & -\delta_2 & 0 & -\delta_3 \\
1 & 0 & 1 & 0 & 1 & 0 \\
0 & -\gamma_1 & 0 & -\gamma_2 & 0 & -\gamma_3 \\
-\delta_1 S_{h_1} & -\delta_1 C_{h_1} & -\delta_2 S_{h_2} & -\delta_2 C_{h_2} & -\delta_3 S_{h_3} & -\delta_3 C_{h_3} \\
C_{h_1} & S_{h_1} & C_{h_2} & S_{h_2} & C_{h_3} & S_{h_3} \\
-\gamma_1 S_{h_1} & -\gamma_1 C_{h_1} & -\gamma_2 S_{h_2} & -\gamma_2 C_{h_2} & -\gamma_3 S_{h_3} & -\gamma_3 C_{h_3}
\end{bmatrix}
\begin{bmatrix} B_1 \\ B_2 \\ B_3 \\ B_4 \\ B_5 \\ B_6 \end{bmatrix}
\tag{34}
$$

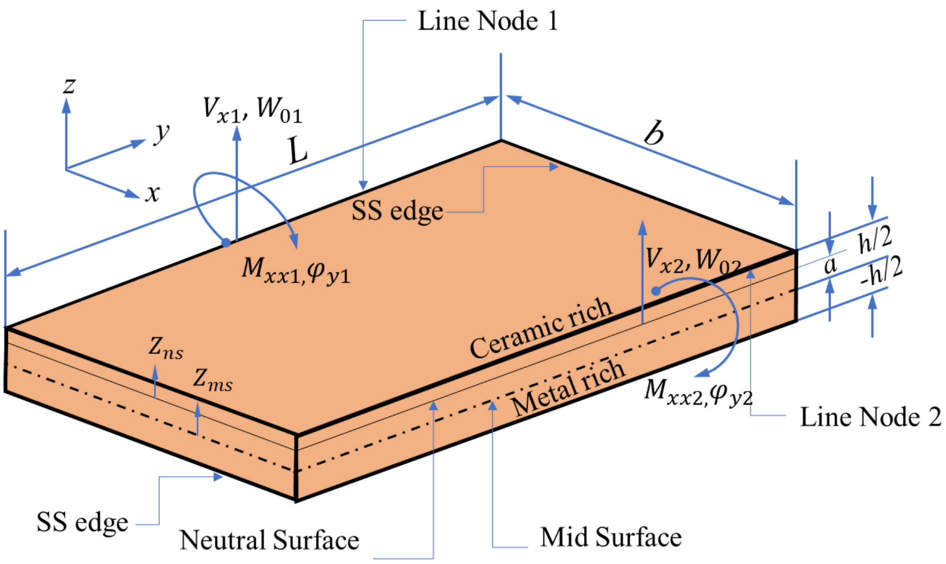

Fig. 2. Boundary (edge) conditions for displacements and forces of a FGM plate

i.e.,

$$\boldsymbol{\delta} = \mathbf{BC} \tag{35}$$

where

$$C_{h_1} = \cosh(\Upsilon_{1m}b), \quad S_{h_1} = \sinh(\Upsilon_{1m}b), \quad C_{h_2} = \cosh(\Upsilon_{2m}b),$$
$$S_{h_2} = \sinh(\Upsilon_{2m}b) \quad C_{h_3} = \cosh(\Upsilon_{3m}b), \quad S_{h_3} = sinh(\Upsilon_{3m}b) \tag{36}$$

Similarly, by substituting the boundary (edge) conditions of Eq. (33) for forces and moments into Eqs. (29)-(31), the following matrix relationship is obtained.

$$\begin{bmatrix} \mathcal{Q}_{x_1} \\ \mathcal{M}_{xx_1} \\ \mathcal{M}_{xy_1} \\ \mathcal{Q}_{x_2} \\ \mathcal{M}_{xx_2} \\ \mathcal{M}_{xy_2} \end{bmatrix} = \begin{bmatrix} \mathcal{L}_1 & 0 & \mathcal{L}_2 & 0 & \mathcal{L}_3 & 0 \\ 0 & \mathcal{R}_1 & 0 & \mathcal{R}_2 & 0 & \mathcal{R}_3 \\ \mathcal{T}_1 & 0 & \mathcal{T}_2 & 0 & \mathcal{T}_3 & 0 \\ -\mathcal{L}_1 C_{h_1} & -\mathcal{L}_1 S_{h_1} & -\mathcal{L}_2 C_{h_2} & -\mathcal{L}_2 S_{h_2} & -\mathcal{L}_3 C_{h_3} & -\mathcal{L}_3 S_{h_3} \\ -\mathcal{R}_1 S_{h_1} & -\mathcal{R}_1 C_{h_1} & -\mathcal{R}_2 S_{h_2} & -\mathcal{R}_2 C_{h_2} & -\mathcal{R}_3 S_{h_3} & -\mathcal{R}_3 C_{h_3} \\ -\mathcal{T}_1 C_{h_1} & -\mathcal{T}_1 S_{h_1} & -\mathcal{T}_2 C_{h_2} & -\mathcal{T}_2 S_{h_2} & -\mathcal{T}_3 C_{h_3} & -\mathcal{T}_3 S_{h_3} \end{bmatrix} \begin{bmatrix} B_1 \\ B_2 \\ B_3 \\ B_4 \\ B_5 \\ B_6 \end{bmatrix} \tag{37}$$

i.e

$$\mathbf{F} = \mathbf{SC} \tag{38}$$

where

$$\mathcal{L}_i = GhK_s(\delta_i\Upsilon_i - 1), \quad \mathcal{R}_i = D^*(\alpha\gamma_i\nu - \Upsilon_i), \quad \mathcal{T}_i = \frac{1}{12}Gh^3(\alpha + \gamma_i\Upsilon_i) \tag{39}$$

with *i*= 1,2, 3

Thus, from Eqs. (35) and (38) the DS matrix **K** for an FGM plate using FSDT is obtained as:

$$\mathbf{F} = \mathbf{K\delta} \tag{40}$$

where

$$\mathbf{K} = \mathbf{SB^{-1}} \tag{41}$$

where, **K** is the required dynamic stiffness matrix.

The twelve independent terms $s_{qq}, s_{qm}, s_{qt}, f_{qq}, f_{qm}, f_{qt}, s_{mm}, s_{mt}, s_{tt}, f_{mm}, f_{mt}, f_{tt}$ of the 6×6 symmetric stiffness matrix form the fundamental basis of the analysis as expressed below.

$$\mathbf{K} = \begin{bmatrix} s_{qq} & s_{qm} & s_{qt} & f_{qq} & f_{qm} & f_{qt} \\ s_{qm} & s_{mm} & s_{mt} & -f_{qm} & f_{mm} & f_{mt} \\ s_{qt} & s_{mt} & s_{tt} & f_{qt} & -f_{mt} & f_{tt} \\ f_{qq} & -f_{qm} & f_{qt} & s_{qq} & -s_{qm} & s_{qt} \\ f_{qm} & f_{mm} & -f_{mt} & -s_{qm} & s_{mm} & -s_{mt} \\ f_{qt} & f_{mt} & f_{tt} & s_{qt} & -s_{mt} & s_{tt} \end{bmatrix} \tag{42}$$

The explicit expressions for each of the terms of the dynamic stiffness matrix **K** are obtained by extensive use of symbolic algebra through the application of MATLAB and they are given in Appendix A. The derivation of these expression might have been impossible without the use of symbolic computation.

Matrix **K** in Eq. (42) is defined as dynamic stiffness matrix for an element and is assembled for whole plate to obtain overall dynamic stiffness matrix.

Assembly procedure of DSM used for FGM plates resembles to that of FEM with the exception that line nodes instead of point nodes are used. Subsequently, the penalty method is applied to boundary (edge) conditions to restrain any degree of freedom. This method suppresses the degree of freedom (DOF) by attaching a very large stiffness to the appropriate leading diagonal term of the assembled dynamic stiffness matrix.

The following procedures are used to apply the restraints, i.e., the boundary (edge) conditions [32].

- Free (F): no penalty is applied.
- Simply supported (SS): transverse displacement (W_i) and bending rotation (φ_{x_i}) is penalized
- Clamped (C): transverse displacement (W_i) and bending rotations (φ_{x_i}) and (φ_{y_i}) are penalized.

where i the node to be constrained.

2.4 Application of the Wittrick –Williams (W-W) algorithm

The W-W algorithm is generally employed for systems with infinite number of degrees of freedom (DOF) involving transcendental function of the frequency as is the case with DSM. The algorithm takes into consideration the Sturm sequence property of the dynamic stiffness matrix when computing the eigenvalues, and it guarantees that no eigenvalues of the structure being analysed, is missed. The W-W algorithm identifies the numbers of natural frequencies of a structure which falls within the range of arbitrary trial frequencies selected by the user. Since the method uses consecutive trial frequencies, bisection method is applied to obtain a high degree of accuracy between the desired ranges of frequencies by establishing the upper and lower bounds of the natural frequencies of the plate. Figure 3 shows the computational steps in the form of a flowchart. The W-W algorithm is extensively elaborated in the literature, see for example Boscolo and Banerjee [32].

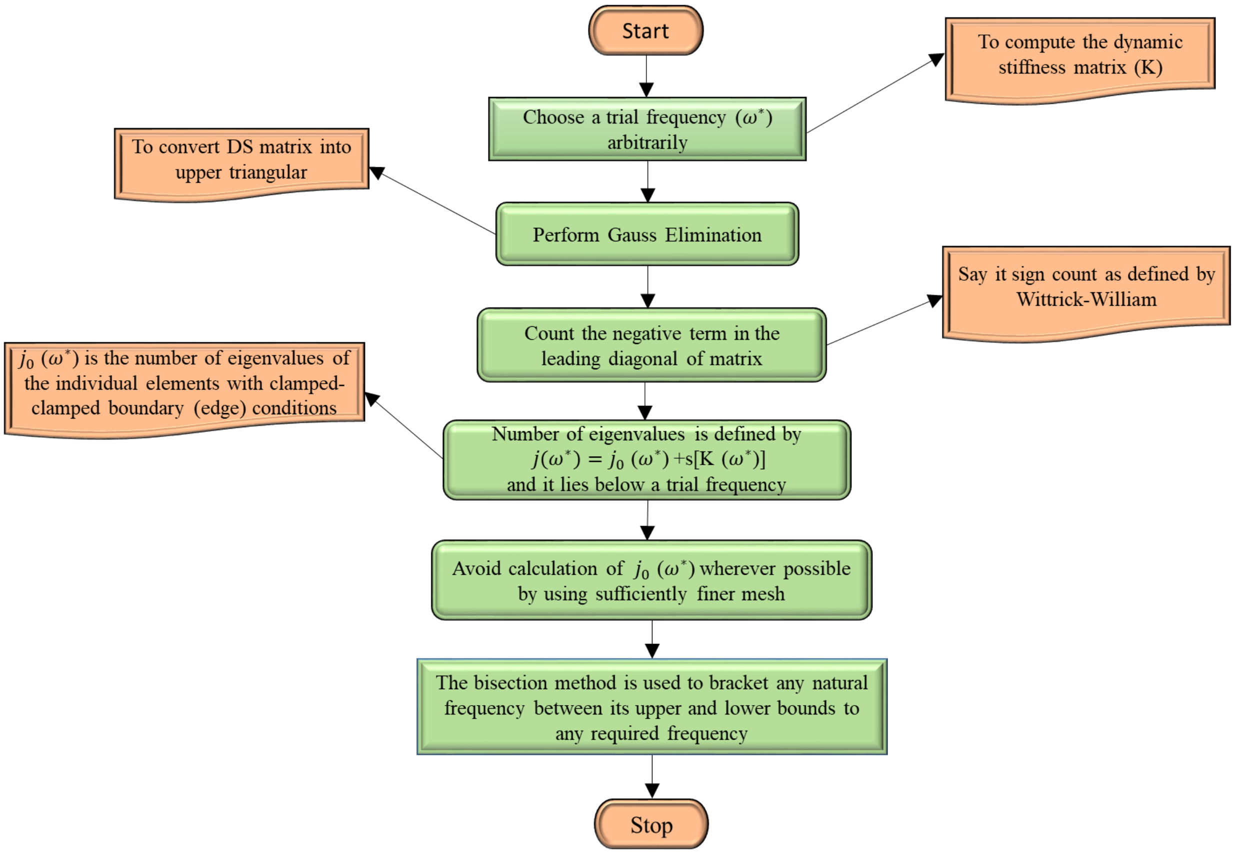

Fig. 3. Computational steps in implementing the Wittrick-Williams algorithm

3. Results and discussion

In order to compute the natural frequencies (eigenvalues) and mode shapes (eigenvectors) of FGM plates using FSDT, a MATLAB program was developed using the above theory and results are presented to demonstrate the significance of the aspect ratio (*L/b*), material gradient index (*k*), thickness to length ratio and boundary (edge) conditions on the natural frequencies and mode shapes.

3.1 Analysis of FGM plates – a comparative study

First, attention is focused on the validation of results computed using the present theory. This is accomplished by comparing results for the isotropic and FGM plates with the ones that are available in the literature. The data for the material properties used in the analysis for the FGM plates are E_c=380 GPa; E_m = 69 GPa; ρ_c =3980 kg/m^3; ρ_m = 2710 kg/m^3 and the non-dimensional natural frequency parameter is defined as $\Omega = (\omega L^2\sqrt{\rho_c/E_c})/h$ which has been here and hereafter, when presenting the results. The degenerate cases when the plate is fully ceramic (E_m= E_c, ρ_m = ρ_c) or fully metallic (E_c=E_m , ρ_c=ρ_m) are investigated in the first instance, for which Hosseini-Hashemi et al. [55] published some results using an exact analytical approach for different h/L ratios of a plate with simply-supported boundary (edge) condition at all edges (SSSS). The results given in Tables 1 and 2 demonstrate the convergence and stability of the present exact approach. Clearly, when the material gradient index (k) approaches zero or infinity (see Eqs. (1)-(3)), the plate behaves as if it is made of an isotropic material, being either fully ceramic or fully metallic. Considering that isotropic materials represent a particular case of FGMs, the first two non-dimensional natural frequencies Ω_1 and Ω_2 computed using the current theory and shown in Tables 1 and 2 are compared with the solutions reported by Hosseini-Hashemi et al. [55], which are also based on the first-order deformation theory. The findings of the current research indicate a consistent trend of monotonic convergence and a very close match with the results of Hosseini-Hashemi et al. [55].

Table 1 Non-dimensional natural frequency parameter Ω_i (i = 1, 2) for a fully ceramic (isotropic) square plate under SSSS boundary (edge) condition.

Sources	k	Ω_1			Ω_2		
		h/L=0.05	h/L =0.1	h/L =0.2	h/L =0.05	h/L =0.1	h/L =0.2
Hosseini-Hashemi et al. [55]	10^{-3}	5.9191	5.7728	5.2954	14.611	13.789	11.612
Present		5.9175	5.7670	5.2782	14.6012	13.7584	11.5412
Hosseini-Hashemi et al. [55]	10^{-4}	5.9212	5.7748	5.2972	14.616	13.794	11.615
Present		5.9196	5.7691	5.2799	14.6064	13.7631	11.54496
Hosseini-Hashemi et al. [55]	10^{-5}	5.9214	5.7751	5.2974	14.616	13.795	11.616
Present		5.9198	5.7693	5.2801	14.6069	13.7636	11.54533
Hosseini-Hashemi et al. [55]	10^{-6}	5.9214	5.7751	5.2974	14.616	13.795	11.616
Present		5.9198	5.7693	5.2801	14.6070	13.7636	11.5453

Table 2 Non-dimensional natural frequency parameter Ω_i (i = 1, 2) for a fully metallic (isotropic) square plate under SSSS boundary (edge) condition.

Sources	k	Ω_1			Ω_2		
		h/L=0.05	h/L =0.1	h/L =0.2	h/L =0.05	h/L =0.1	h/L =0.2
Hosseini-Hashemi et al. [55]	10^2	3.1833	3.1002	2.8315	7.8518	7.3875	6.1756
Present		3.1823	3.0968	2.8217	7.8464	7.3700	6.1363
Hosseini-Hashemi et al. [55]	10^3	3.0329	2.9575	2.7115	7.4858	7.0622	5.9416
Present		3.0320	2.9544	2.7025	7.4809	7.0464	5.9055
Hosseini-Hashemi et al. [55]	10^4	3.0158	2.9413	2.6978	7.4443	7.0254	5.9152
Present		3.0150	2.9383	2.6890	7.4394	7.0096	5.8793
Hosseini-Hashemi et al. [55]	10^5	3.0139	2.9394	2.6963	7.4396	7.0212	5.9123
Present		3.0133	2.9366	2.6877	7.4352	7.0059	5.8767

In the second example, the first four non-dimensional frequency parameters Ω_i (i =1, 2, 3, 4) of a rectangular P-FG plate under SSSS boundary (edge) condition and for different h/L ratio and material gradient index k, computed by the present theory are shown in Table 3, together with the results reported by Hosseini-Hashemi et al. [55]. Clearly, the results obtained from the present theory are in complete agreement with the results reported in [55].

Table 3 Non-dimensional natural frequency parameter Ω_i (i=1, 2, 3, 4) for a rectangular P-FG plate under SSSS boundary (edge) condition at L/b=2 and for different h/L values

h/L	Ω_i	Sources	SSSS						
			k=0	k=0.5	k=1	k =2	k=5	k =8	k=10
0.05	Ω_1	Hosseini-Hashemi et al. [55]	3.7123	3.1456	2.8352	2.5777	2.4425	2.3948	2.3642
		Present	3.7123	3.1456	2.8352	2.5777	2.4424	2.3947	2.3642
	Ω_2	Hosseini-Hashemi et al. [55]	5.9198	5.0175	4.5228	4.1115	3.8939	3.8170	3.7681
		Present	5.9198	5.0175	4.5228	4.1115	3.8939	3.8170	3.7681
	Ω_3	Hosseini-Hashemi et al. [55]	9.5668	8.1121	7.3132	6.6471	6.2903	6.1639	6.0843
		Present	9.5668	8.1121	7.3132	6.6471	6.2903	6.1639	6.0843
	Ω_4	Hosseini-Hashemi et al. [55]	12.4561	10.566	9.5261	8.6572	8.1875	8.0207	7.9166
		Present	12.4561	10.5656	9.5261	8.6573	8.1875	8.0207	7.9165
0.1	Ω_1	Hosseini-Hashemi et al. [55]	3.6518	3.0983	2.7937	2.5386	2.3998	2.3504	2.3197
		Present	3.6517	3.0983	2.7936	2.5386	2.3998	2.3504	2.3197
	Ω_2	Hosseini-Hashemi et al. [55]	5.7693	4.8997	4.4192	4.0142	3.7881	3.7072	3.6580
		Present	5.7693	4.8997	4.4192	4.0142	3.7881	3.7072	3.6580
	Ω_3	Hosseini-Hashemi et al. [55]	9.1876	7.8145	7.0512	6.4015	6.0247	5.8887	5.8086
		Present	9.1876	7.8145	7.0513	6.4017	6.0249	5.8889	5.8088
	Ω_4	Hosseini-Hashemi et al. [55]	11.831	10.074	9.0928	8.2515	7.7505	7.5688	7.4639
		Present	11.8306	10.0737	9.0930	8.2519	7.7511	7.5693	7.4643
0.2	Ω_1	Hosseini-Hashemi et al. [55]	3.4409	2.9322	2.6473	2.4017	2.2528	2.1985	2.1677
		Present	3.4409	2.9322	2.6474	2.4018	2.2530	2.1987	2.1678
	Ω_2	Hosseini-Hashemi et al. [55]	5.2802	4.5122	4.0773	3.6953	3.4492	3.3587	3.3094
		Present	5.2802	4.5123	4.0777	3.6959	3.4500	3.3593	3.3099
	Ω_3	Hosseini-Hashemi et al. [55]	8.0710	6.9231	6.2636	5.6695	5.2579	5.1045	5.0253
		Present	8.0709	6.9236	6.2648	5.6715	5.2602	5.1063	5.0268
	Ω_4	Hosseini-Hashemi et al. [55]	9.7416	8.6926	7.8711	7.1189	6.5749	5.9062	5.7518
		Present	10.1089	8.6934	7.8731	7.1224	6.5788	6.3738	6.2709

In the third example, the fundamental non-dimensional natural frequency parameter ($\hat{\beta}$) of a square P-FG plate defined by $\hat{\beta} = \omega_1 h\sqrt{\rho_m/E_m}$ under SSSS boundary (edge) condition is computed by the present method for different values of k and thickness to length (*h/L*) ratio and the results are shown in Table 4 alongside the results reported by Matsunaga [82], Vel and Batra [83], Pradyumna and Bandyopadhyay [84] and Hosseini-Hashemi et al. [55, 57] which are respectively based on HSDT, 3-dimensional elasticity theory via power series method, FSDT by using FEM, FSDT via analytical solutions and Reissner-Mindlin plate theory via analytical solutions. The fundamental natural frequency computed by the present method agrees very well with results available in the literature, as can be seen in Table 4.

Table 4 Non-dimensional fundamental natural frequency parameter $\hat{\beta} = \omega_1 h\sqrt{\rho_m/E_m}$ for a square P-FG plate for different *h/L* ratios and material gradient index *k*, under SSSS boundary (edge) condition.

Source	*k*=0		*k*=1			*h/L*=0.2		
	h/L=0.316	*h/L*=0.1	*h/L=0.05*	*h/L=0.1*	*h/L=0.2*	*k*=2	*k*=3	*k*=5
Matsunaga [82]	0.4619	0.0577	0.0162	0.0633	0.2323	0.2325	0.2334	0.2334
Vel and Batra [83]	0.4658	0.0578	0.0157	0.0613	0.2257	0.2237	0.2243	0.2253
Pradyumna and Bandyopadhyay [84]	0.4658	0.0577	0.0158	0.0619	0.2285	0.2264	0.2270	0.2281
Hosseini-Hashemi et al. [57]	0.4618	0.0576	0.0158	0.0611	0.2270	0.2249	0.2254	0.2265
Hosseini-Hashemi et al. [55]	0.4618	0.0577	0.0158	0.0619	0.2276	0.2264	0.2276	0.2291
Present	0.4618	0.0578	0.0158	0.0619	0.2276	0.2264	0.2276	0.2291

3.2 Free vibration analysis of P-FG plates using the proposed DSM based on FSDT

The next set of results was obtained for a square plate with isotropic and P-FG material properties and with SSSS, SFSS, SFSF, SFSC and SCSC boundary (edge) conditions which all render to the Levy type of solution. (Note that the letters S, F and C correspond to simple-support, free and clamped boundary (edge) conditions, respectively at the edge of the plate written in a sequential clockwise or anticlockwise manner). Tables 5 and 6 show the first six non-dimensional natural frequency parameter Ω_i (i=1, 2, 3, 4, 5, 6) of the square isotropic and P-FG plate, respectively by using the present approach. The results for the isotropic plate (material gradient index k=0) are shown in Table 5 whereas the results for the P-FG plate with material gradient index k=0.5 are shown in Table 6. When computing the results of both Tables 5 and 6 results, the thickness to length ratio was taken to be h/L=0.2 whereas the value of the material index k was set to 0 for the isotropic plate and 0.5 for the P-FG plate, respectively. As expected, the natural frequency parameter for both the isotropic and FGM plates are highest for SCSC boundary (edge) condition and lowest for SFSF boundary (edge) conditions.

Table 5 First six non-dimensional natural frequency parameter Ω_i (i=1, 2, 3, 4, 5, 6) of a square isotropic plate under different boundary (edge) conditions at $h/L=0.2$ and k=0.

BCs	Ω_1	Ω_2	Ω_3	Ω_4	Ω_5	Ω_6
SFSF	3.2038	6.9042	9.8747	13.0359	13.6057	18.3567
SSSF	3.2374	7.0064	9.9002	13.1861	13.7099	18.3798
SCSF	3.4382	7.7936	9.9541	13.5342	14.6775	18.3973
SSSS	5.2801	11.5453	11.5453	16.6891	19.7138	19.7138
SCSS	5.9624	11.7859	12.5425	17.1994	19.8048	20.5585
SCSC	6.7662	12.0599	13.5012	17.7180	19.9030	21.3531

Table 6 First six non-dimensional natural frequency parameter Ω_i (i=1, 2, 3, 4, 5, 6) of square P-FG plate under different boundary (edge) condition at $h/L=0.2$ and k=0.5

BCs	Ω_1	Ω_2	Ω_3	Ω_4	Ω_5	Ω_6
SFSF	2.7311	5.9117	8.4890	11.2411	11.7189	15.9176
SSSF	2.7585	5.9966	8.5107	11.3701	11.8077	15.9307
SCSF	2.9342	6.7028	8.5597	11.6924	12.7098	19.8448
SSSS	4.5123	9.9449	9.9449	14.4496	17.1128	17.1128
SCSS	5.1190	10.1666	10.8668	14.9328	17.1994	17.9300
SCSC	5.8412	10.4215	11.7613	15.4269	17.2935	18.6998

Next, the non-dimensional fundamental frequency parameter Ω_1 of a moderately thick P-FG plate is presented in Table 7 for different values of b/L (0.5, 1, 1.5, 2, and 2.5) and k (0, 0.5, 1, 2, and 5) under SFSF, SSSF, SCSF, SSSS, SCSS and SCSC boundary (edge) conditions. One can notice from Table 7 that the fundamental frequency parameter decreases with an increase in the b/L value, when all other parameters of the plate are taken to be constant. It is also found that the fundamental frequency parameter of the plate increases as the constraint on the boundary (edge) of the plate increases (from free F, to simply supported SS and to clamped C). Table 7 also depicts that the frequency parameter decreases as the value of the material gradient index increases. This is because, at higher values of k, the P-FG plate contains fewer ceramic constituents, leading to a reduction in stiffness.

Table 7 Non-dimensional fundamental natural frequency parameter Ω_1 for a rectangular P-FG plate for different boundary (edge) conditions and different values of *b/L* and *k* with *h/L*=0.1

b/L	*k*	Boundary (edge) conditions					
		SFSF	SSSF	SCSF	SSSS	SCSS	SCSC
0.5	0	11.0021	11.5858	11.6912	13.7636	14.2543	14.8622
	0.5	9.3658	9.8654	9.9573	11.7290	12.1583	12.6933
	1	8.4533	8.9048	8.9887	10.5897	10.9820	11.4723
	2	7.6718	8.0807	8.1565	9.6075	9.9625	10.4060
	5	7.2093	7.5899	7.6583	9.0120	9.3313	9.7267
1	0	2.8568	3.4416	3.7067	5.7693	6.7751	8.0702
	0.5	2.4232	2.9205	3.1475	4.8997	5.7649	6.8848
	1	2.1848	2.6335	2.8390	4.4192	5.2040	6.2223
	2	1.9856	2.3929	2.5794	4.0142	4.7261	5.6495
	5	1.8779	2.2615	2.4351	3.7881	4.4463	5.2932
1.5	0	1.2730	1.8088	2.1974	4.2058	5.4524	7.0187
	0.5	1.0789	1.5339	1.8650	3.5693	4.6375	5.9866
	1	0.9725	1.3829	1.6820	3.2186	4.1860	5.4106
	2	0.8841	1.2570	1.5286	2.9244	3.8025	4.9136
	5	0.8373	1.1893	1.4444	2.7632	3.5801	4.6057
2	0	0.7154	1.1996	1.6819	3.6517	5.0123	6.6912
	0.5	0.6062	1.0171	1.4271	3.0983	4.2626	5.7066
	1	0.5463	0.9169	1.2870	2.7936	3.8474	5.1574
	2	0.4967	0.8335	1.1697	2.5386	3.4952	4.6841
	5	0.4707	0.7889	1.1058	2.3998	3.2918	4.3916
2.5	0	0.4574	0.8950	1.4494	3.3940	4.8147	6.5487
	0.5	0.3875	0.7588	1.2295	2.8793	4.0942	5.5846
	1	0.3492	0.6841	1.1087	2.5961	3.6953	5.0471
	2	0.3175	0.6218	1.0078	2.3592	3.3572	4.5841
	5	0.3010	0.5887	0.9530	2.2307	3.1623	4.2985

It would now be instructive to show the influence of the material gradient index on the fundamental natural frequency parameter Ω_1 of the plate. Figure 4 shows this effect for the P-FG plate of the above example with SSSS boundary (edge) condition for different *h/L* ratios. It can be seen from Fig. 4 that Ω_1 decreases with increasing values of *k*. However, when $k < 2$, the fundamental natural frequency decreases much more rapidly than when $k>2$. It can also be observed that the material inhomogeneity effect of the material characteristics of the FGM plate on the fundamental natural frequency becomes more pronounced when the thickness of the plate increases.

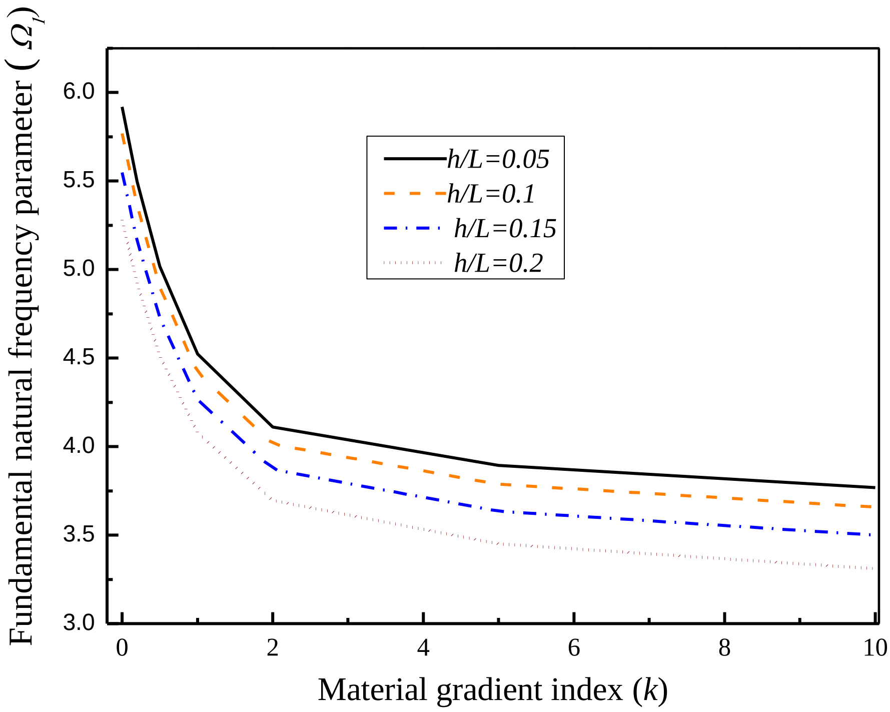

Fig. 4. The influence of material gradient index (*k*) on the Ω_1 for square P-FG plate at different *h/L* ratios under SSSS boundary (edge) condition.

Figure 5 shows the variation of the non-dimensional fundamental natural frequency Ω_1 of the square P-FG plate with SSSS boundary (edge) condition with respect to the *h/L* ratio, for different values of *k*. It may be noted that the variation of Ω_1 shows similar trends for all the *k* values shown i.e. decrease in the fundamental natural frequency with higher thickness to length ratio. While the actual natural frequency (ω) increases with the increase in thickness (*h*) due to increased stiffness, the non-dimensional natural frequency parameter $\Omega = (\omega L^2\sqrt{\rho_c/E_c})/h$ decreases because it includes a factor of 1/*h* in the denominator. In other words, ω does not increase fast enough to offset the consequence of the division by *h* in Ω, and therefore in the plotted results in Fig. 5, the non-dimensional natural frequency drops with increasing values of *h/L*.

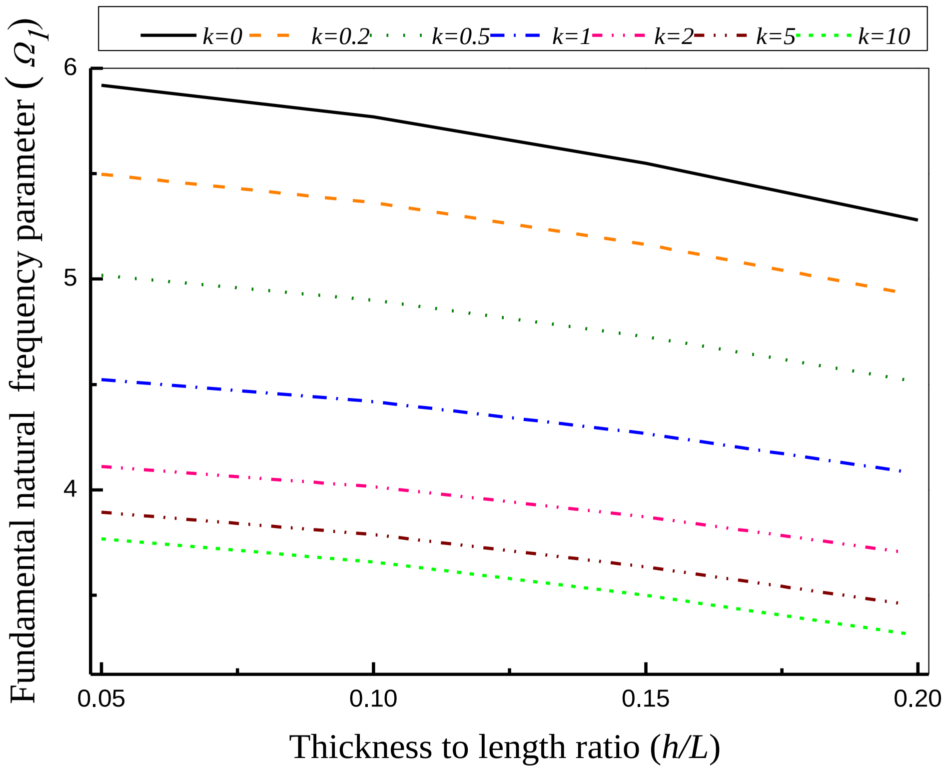

Fig. 5. The influence of thickness to length ratio (*h/L*) on the Ω_1 for square P-FG plate at different values of *k* under SSSS boundary (edge) condition.

The variations of the non-dimensional natural frequency parameter Ω_i (i=1, 2, 3, 4, 5, 6) with thickness to length ratio *h/L* for a given *L/b*=1 and *k*=0.5 are shown in Fig. 6 for the SSSS boundary (edge) condition. The figure shows that with the increase in the *h/L* ratio the non-dimensional natural frequency parameter Ω_i decreases. As the thickness-to-length ratio (*h/L*) increases, the non-dimensional frequency parameter (Ω_i) decreases due to its inverse dependence on the thickness (*h*). While an increase in *h* enhances the bending stiffness, leading to a rise in the natural frequency (ω_i), the effect of *h* in the denominator of Ω_i is stronger because $\Omega_i = (\omega_i L^2 \sqrt{\rho_c / E_c})/h$. Thus, the increase in ω_i is not sufficient to compensate for the division by *h* in the expression for Ω, resulting in an overall decrease in Ω as *h/L* grows.

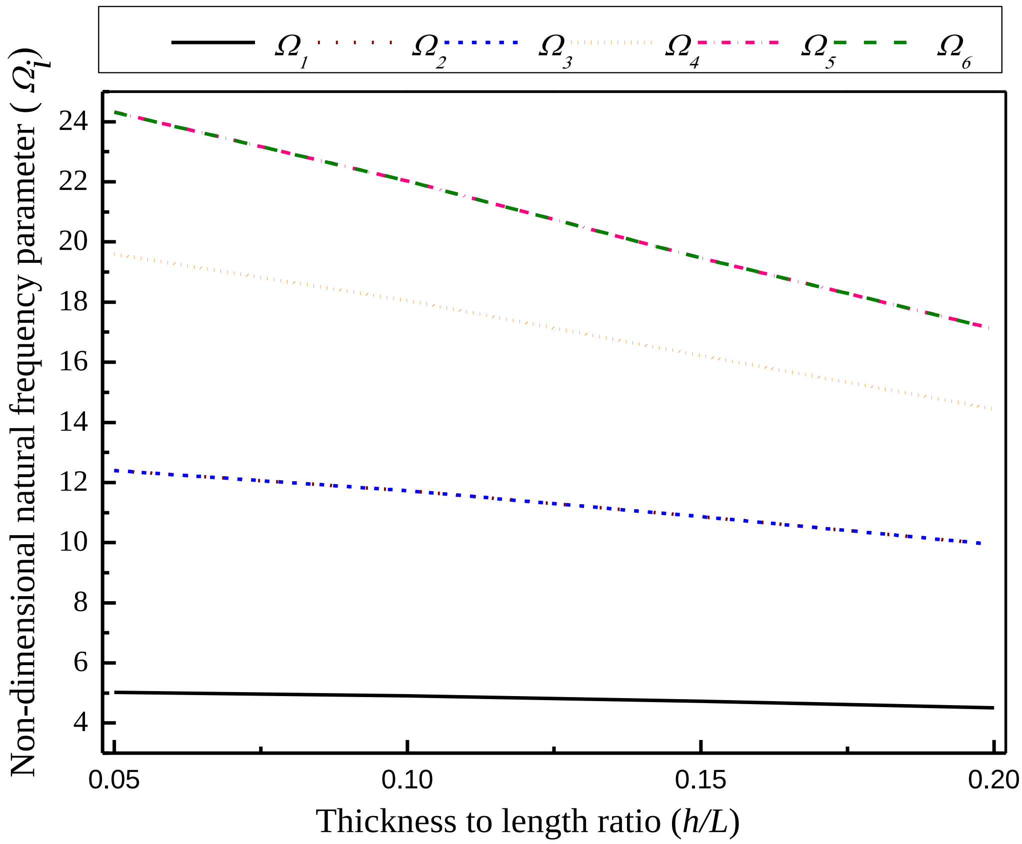

Fig. 6. The variation of the first six non-dimensional frequency parameter Ω_i (i=1, 2, 3, 4, 5, 6) against the thickness to length ratio (*h/L*) of the square FGM plate for *k*=0.5 and for SSSS boundary (edge) condition.

The effects of material gradient index and boundary (edge) conditions on the fundamental natural frequency parameter of the square P-FG plate are shown in Fig. 7. As expected, there is an increase in the fundamental natural frequency parameter when the constraints at the boundaries are increased so that the fundamental natural frequency parameter of the SFSF boundary (edge) condition has the lowest value whereas that of the SCSC case has the highest value.

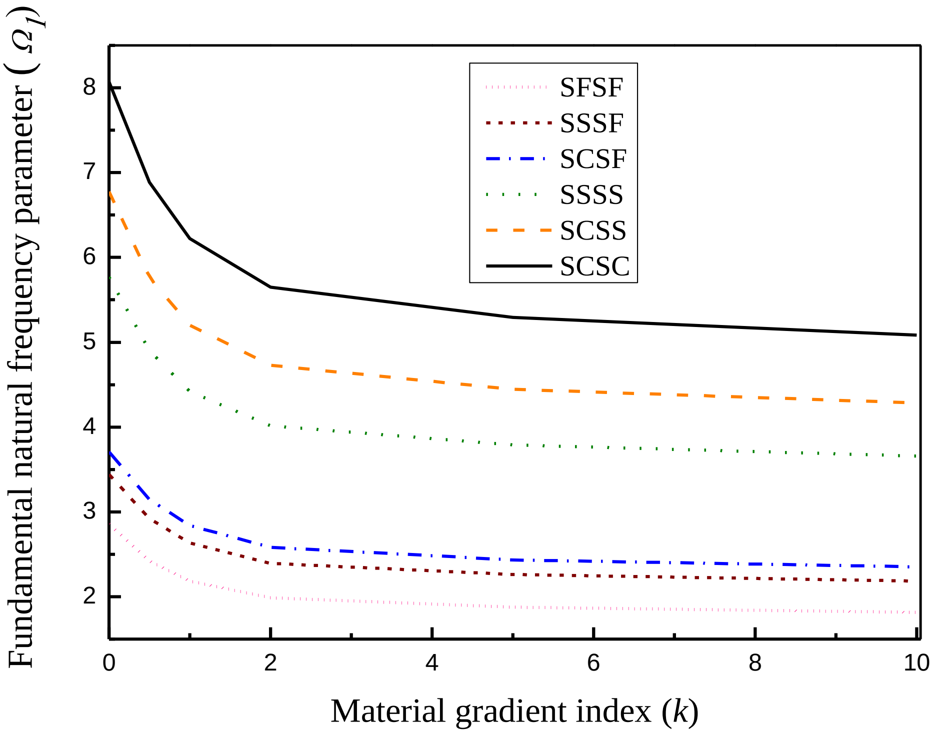

Fig. 7. Non-dimensional fundamental natural frequency parameter Ω_1 versus the material gradient index (k) of the square P-FG plate for h/L = 0.1 under different boundary (edge) conditions.

The mode shapes of the P-FG square plate for the SSSS boundary (edge) condition using the present theory for L/b=1, h/L=0.05, k=0.5 are illustrated in Fig.8. They follow more or less very similar trends as observed in isotropic plates, but the natural frequencies are markedly different.

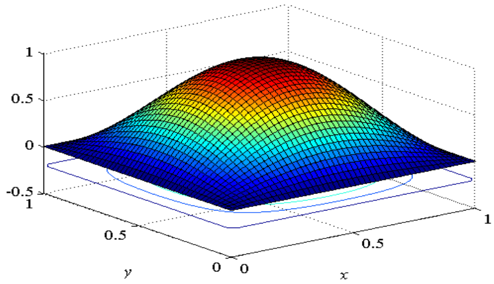

Natural mode (m=1, n=1)

$\Omega_1 = 0.000476$

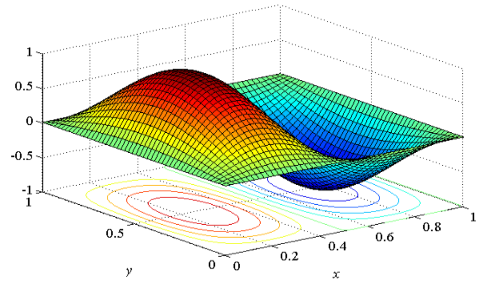

Natural mode (m=1, n=2)

$\Omega_2 = 0.001192$

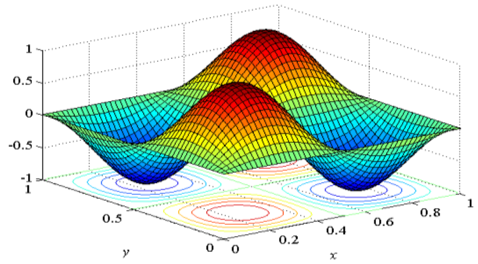

Natural mode (m=2, n=2)

$\Omega_3 = 0.001096$

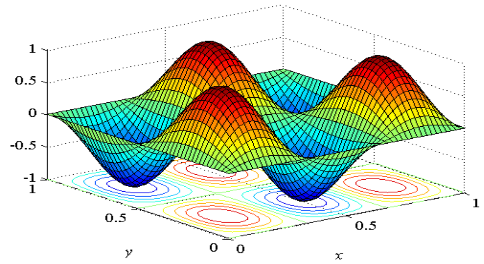

Natural mode (m=2, n=3)

$\Omega_4 = 0.003101$

Fig. 8. Natural mode shapes of P-FG square plate under SSSS boundary (edge) condition for k=0.5 and h/L=0.01 via FSDT.

3.3 Natural vibration of S-FG plate

Now, some results for the S-FG plates are presented in this section. Table 8 shows the first six non-dimensional natural frequency parameter Ω_i (i=1, 2, 3, 4, 5, 6) for a square S-FG plate based on the present approach under Levy-type boundary (edge) conditions (SSSS, SFSS, SFSF, SFSC, SSSC and SCSC).

Table 8 First six non-dimensional natural frequency parameter Ω_i (i=1, 2, 3, 4, 5, 6) of square S-FG plate under different boundary (edge) conditions at $h/L=0.2$ and k=0.5.

BCs	Ω_1	Ω_2	Ω_3	Ω_4	Ω_5	Ω_6
SFSF	2.1790	3.4237	7.0869	7.6310	8.7808	12.1190
SSSF	2.5965	5.6337	7.9859	10.6563	11.0662	15.2817
SCSF	2.7606	6.2880	8.0311	10.9521	11.8933	15.7318
SSSS	4.2431	9.3263	9.3263	13.5280	16.0081	16.0081
SCSS	4.8071	9.5302	10.1739	13.9691	16.0871	16.7498
SCSC	5.4766	9.7641	10.9941	14.4195	16.1726	18.6998

It is obvious from Table 8 that the frequency parameter for S-FG plate under different boundary (edge) conditions follows more or less a similar trend as observed in P-FG plates (see Table 6), but the values of frequency parameter are markedly different, due to variations in the material properties.

Tables 9-11 show the first six non-dimensional natural frequency parameters Ω_i (i=1, 2, 3, 4, 5, 6) for different values of material gradient index (k=0, 0.2, 0.5, 1, 2, 5 and 10) of a S-FG plate based on the present approach when three different boundary (edge) conditions (SSSS, SCSC and SFSF) are applied. For all the three boundary (edge) conditions, the plate is assumed to be square (aspect ratio L/b=1) with three thickness to length ratios of 0.05, 0.1 and 0.2. The following points can be made from the results shown in Tables 9-11.

(i) Frequency parameters are reduced significantly with the increase in the thickness to length ratio, irrespective of edge constraints, material gradient index, or mode numbers. The influence of h/L ratio becomes more substantial for higher modes of vibration. This behaviour is due to the effect of shear deformation and rotary inertia.

(ii) For all three combinations of boundary (edge) conditions, as the values of material gradient index increases, the frequency parameter decreases, keeping all other parameters constant.

Table 9 First six non-dimensional natural frequency parameter Ω_i (i=1, 2, 3, 4, 5, 6) for square S-FG plate for different h/L ratios and k values under SFSF boundary (edge) condition.

h/L	Modes	Material gradient index (k)						
		0	0.2	0.5	1	2	5	10
0.05	Ω_1	2.4106	2.3854	2.3159	2.2130	2.0935	1.9860	1.9531
	Ω_2	3.9920	3.9507	3.8367	3.6678	3.4714	3.2948	3.2406
	Ω_3	8.9923	8.9000	8.6450	8.2668	7.8267	7.4306	7.3090
	Ω_4	9.6177	9.5190	9.2460	8.8411	8.3698	7.9454	7.8151
	Ω_5	11.452	11.3360	11.0132	10.5340	9.9759	9.4729	9.3184
	Ω_6	17.0782	16.9065	16.4312	15.7249	14.9010	14.1574	13.9288
0.1	Ω_1	2.3767	2.3523	2.2849	2.1849	2.0684	1.9636	1.9314
	Ω_2	3.8743	3.8354	3.7277	3.5678	3.3812	3.2129	3.1611
	Ω_3	8.5243	8.4404	8.2080	7.8620	7.4574	7.0915	6.9789
	Ω_4	9.1529	9.0645	8.8194	8.4533	8.0240	7.6345	7.5144
	Ω_5	10.7731	10.6707	10.3863	9.9613	9.4620	9.0083	8.8683
	Ω_6	15.6455	15.5015	15.1012	14.5010	13.7935	13.1481	12.9485
0.2	Ω_1	2.2615	2.2396	2.1790	2.0886	1.9825	1.8862	1.8565
	Ω_2	3.5482	3.5152	3.4238	3.2868	3.1256	2.9788	2.9335
	Ω_3	7.3351	7.2696	7.0870	6.8125	6.4878	6.1907	6.0986
	Ω_4	7.8724	7.8089	7.6310	7.3607	7.0363	6.7356	6.6416
	Ω_5	9.0530	8.9814	8.7808	8.4754	8.1085	7.7676	7.6610
	Ω_6	12.4770	12.3831	12.1190	11.7151	11.2268	10.7706	10.6275

Table 10 First six non-dimensional natural frequency parameter Ω_i (i=1, 2, 3, 4, 5, 6) for square S-FG plate for different h/L ratios and k values under SSSS boundary (edge) condition.

h/L	Modes	Material gradient index (k)						
		0	0.2	0.5	1	2	5	10
0.05	Ω_1	4.9249	4.8737	4.7323	4.5228	4.2793	4.0604	3.9932
	Ω_2	12.1519	12.0278	11.6844	11.1747	10.5811	10.0461	9.8819
	Ω_3	12.1519	12.0278	11.6844	11.1747	10.5811	10.0462	9.8819
	Ω_4	19.1985	19.0055	18.4713	17.6768	16.7497	15.9126	15.6552
	Ω_5	23.8019	23.5651	22.9093	21.9330	20.7921	19.7607	19.4433
	Ω_6	23.8019	23.5651	22.9093	21.9330	20.7921	19.7607	19.4433
0.1	Ω_1	4.7996	4.7514	4.6178	4.4192	4.1874	3.9782	3.9138
	Ω_2	11.4503	11.3418	11.0405	10.5898	10.0597	9.5777	9.4288
	Ω_3	11.4503	11.3418	11.0405	10.5898	10.0597	9.5777	9.4288
	Ω_4	17.5708	17.4128	16.9728	16.3109	15.5275	14.8104	14.5881
	Ω_5	21.4084	21.2220	20.7017	19.9167	18.9838	18.1265	17.8601
	Ω_6	21.4084	21.2220	20.7017	19.9167	18.9838	18.1265	17.8601
0.2	Ω_1	4.3927	4.3532	4.2432	4.0777	3.8819	3.7026	3.6470
	Ω_2	9.6049	9.5318	9.3263	9.0120	8.6321	8.2772	8.1658
	Ω_3	9.6049	9.5318	9.3263	9.0120	8.6321	8.2772	8.1658
	Ω_4	13.8841	13.7912	13.5280	13.1202	12.6192	12.1437	11.9931
	Ω_5	16.4004	16.2984	16.0082	15.5551	14.9935	14.4554	14.2841
	Ω_6	16.4004	16.2984	16.0082	15.5551	14.9935	14.4554	14.2841

Table 11 First six non-dimensional natural frequency parameter Ω_i (i=1, 2, 3, 4, 5, 6) for square S-FG plate for different h/L ratios and k values under SCSC boundary (edge) condition.

h/L	Modes	Material gradient index (k)						
		0	0.2	0.5	1	2	5	10
0.05	Ω_1	7.1274	7.0551	6.8554	6.5585	6.2125	5.9003	5.8044
	Ω_2	13.3648	13.2304	12.8583	12.3050	11.6596	11.0768	10.8977
	Ω_3	16.6796	16.5164	16.0642	15.3898	14.6003	13.8850	13.6646
	Ω_4	22.5455	22.3269	21.7206	20.8160	19.7557	18.7942	18.4978
	Ω_5	24.5236	24.2818	23.6118	22.6135	21.4459	20.3891	20.0637
	Ω_6	30.1711	29.8881	29.1019	27.9247	26.5392	25.2776	24.8878
0.1	Ω_1	6.7138	6.6520	6.4801	6.2223	5.9184	5.6411	5.5553
	Ω_2	12.3642	12.2522	11.9404	11.4723	10.9193	10.4139	10.2574
	Ω_3	14.9062	14.7837	14.4410	13.9218	13.3014	12.7279	12.5491
	Ω_4	19.8413	19.6799	19.2287	18.5445	17.7264	16.9696	16.7335
	Ω_5	21.8631	21.6766	21.1559	20.3690	19.4321	18.5694	18.3011
	Ω_6	25.5204	25.3336	24.8080	24.0038	23.0306	22.1195	21.8332
0.2	Ω_1	5.6290	5.5890	5.4766	5.3046	5.0963	4.9010	4.8396
	Ω_2	10.0329	9.9625	9.7641	9.4594	9.0890	8.7408	8.6310
	Ω_3	11.2320	11.1700	10.9941	10.7199	10.3799	10.0532	9.9488
	Ω_4	14.7401	14.6566	14.4195	14.0496	13.5909	13.1505	13.0099
	Ω_5	16.5578	16.4576	16.1727	15.7275	15.1747	14.6444	14.4752
	Ω_6	17.7641	17.6822	17.4482	17.0793	16.6150	16.1620	16.0158

For illustrative purposes, four representative mode shapes of an S-FG square plate based on FSDT, subjected to SFSS boundary (edge) condition for *h/L*=0.05, *k*=0.5, are presented in Fig. 9. They follow more or less similar trends as observed in isotropic plates, but the natural frequencies are notably different.

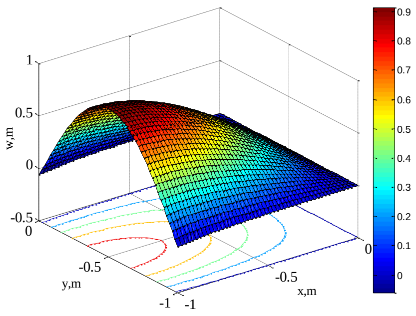

Natural mode (m=1, n=1)

$\Omega_1 = 0.000299$

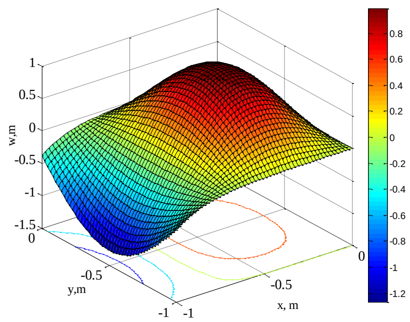

Natural mode (m=1, n=2)

$\Omega_2 = 0.000711$

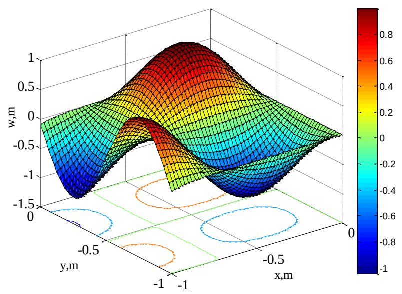

Natural mode (m=2, n=2)

$\Omega_3 = 0.001513$

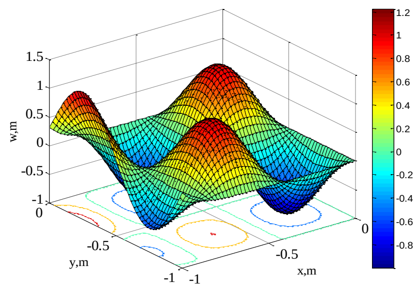

Natural mode (m=2, n=3)

$\Omega_4 = 0.00242$

Fig. 9. Mode shapes of S-FG square plate under SFSS boundary (edge) condition for *k*=0.5 and *h/L*=0.01 via FSDT.

To demonstrate the accuracy and computational efficiency of the proposed Dynamic Stiffness Method (DSM), the example of a square P-FG plate is chosen. In a consistent set of units, the plate has the dimensions a = b =1, thickness h=0.01, giving a thickness ratio of h/a=0.01. The plate is simply supported along all its four edges (SSSS boundary condition). It is made of aluminium oxide (Al_2O_3) and aluminium (Al) and graded through the thickness by using power-law distribution. The accuracy of results for the first five natural frequencies using the proposed DSM using 80 elements is shown in Table 12 alongside the results using FEM with 20,000 elements and the results using classical (analytical) solution with 30 terms in the series. The number of elements and terms in the series were chosen in a way so that the results become directly comparable (the deviation in the results is around 0.05Hz). The superiority of the proposed DSM over FEM is evident, as can be seen in the table, bearing in mind that the classical theory which has very limited applicability is always expected to do better.

Table 12 Accuracy comparison for the first five natural frequencies of a P-FG plate with SSSS boundary condition using DSM, FEM and classical (analytical) methods. (NEL is the number of elements used, NST is the number of series terms)

Frequency No (i)	$f_i = \omega_i/2\pi$ (Hz)		
	DSM (current method) NEL= 80	FEM NEL=20000	Classical (Analytical) Method (NST = 30)
1	60.01	60.03	60.00
2	140.02	140.05	140.00
3	240.05	240.10	240.00
4	370.10	370.15	370.00
5	510.12	510.20	510.00

The computational efficiency of the proposed DSM when computing the natural frequencies of the above P-FG plate was assessed by the estimates of CPU time when compared with FEM and classical (analytical) method. Figure 10 shows the comparison of CPU time using the three methods with reference to the computed results shown in Table 12. Although the analytical method is the fastest (0.35s), but it should be recognised that its applicability is limited and often restricted to a single plate. The CPU time for DSM follows closely with CPU time of 0.45s, offering a strong balance between speed and general applicability. By contrast, FEM is significantly slower with CPU time 1.75s due to its computationally intensive mesh handling to achieve comparable results. The results of Table 12 and Fig. 10 reveal that the proposed DSM stands out as a highly efficient and accurate tool for free vibration analysis of moderately thick FGM plates.

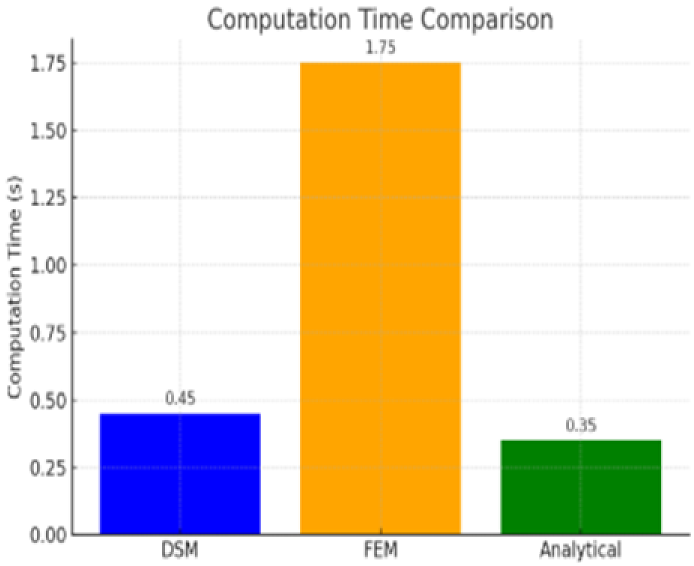

Fig. 10. Comparison of CPU time using DSM, FEM and classical (analytical) method

4. Conclusions

- The free vibration behaviour of moderately thick functionally graded material (FGM) plates, following power-law (P-FG) and sigmoid-law (S-FG) distributions, has been investigated using the Dynamic Stiffness Method (DSM) for the first time.
- The DSM is proved to be very effective to analyze moderately thick FGM plates accurately, for which the finite element method (FEM) can sometimes become inadequate, particularly at the high frequency range.
- The formulation is based on the First-Order Shear Deformation Theory (FSDT), which captures transverse shear deformation and rotatory inertia effects essential for moderately thick plate analysis.
- The dynamic stiffness matrix is solved using the Wittrick–Williams algorithm, ensuring that all natural frequencies are accurately and efficiently identified.
- The accuracy of the present DSM-based method is validated by comparing results with those from the literature, showing excellent agreement with existing analytical and numerical results.

- A comprehensive parametric study was conducted by varying:

    (i) Aspect ratio (*L/b*),
    (ii) Thickness-to-length ratio (*h/L*),
    (iii) Material gradient index (*k*),
    (iv) Boundary (edge) conditions.

- This study highlights the significant influence of above parameters on the free vibration characteristics of P-FG and S-FG plates.
- DSM has shown superior performance, especially for higher modes, where conventional finite element methods (FEM) may lose accuracy.
- The results provided serve as benchmark solutions for future researchers using FEM or other approximate methods.
- Limitations of the current study include:

    (i) The FSDT-based model may be less accurate for very thick plates, where higher-order theories like HSDT or TSDT may be more appropriate.
    (ii) Additionally, for large values of the material gradient index (*k*), extreme material property gradients may affect numerical stability and accuracy.
    (iii) Future work may focus on extending the present framework using higher-order shear deformation theories or refined DSM formulations for better accuracy and stability in extreme material gradation cases.

- The main contribution made in this paper lies in the fact that the DSM has been applied for the first time in the context of moderately thick FGM plates which follow power and sigmoid laws in the property distribution through the thickness.
- The results presented can be used as an aid to validate finite element and other approximate methods.

Appendix-A

Explicit algebraic expressions for the elements of the dynamic stiffness matrix of Eq. (42):

$$S_{qq} = \frac{Ghk}{\Delta}\Big\{-\Big(C_{h_3}\Big(\gamma_1\delta_3(\Upsilon_2\gamma_2\delta_2 + \Upsilon_3\gamma_3\delta_2 - 2\Upsilon_3\gamma_2\delta_3) + \delta_1\Big(-\Big((\Upsilon_1\gamma_1 + \Upsilon_2\gamma_2)\gamma_3\delta_2\Big) + \gamma_2(\Upsilon_1\gamma_1 + \Upsilon_3\gamma_3)\delta_3\Big) + S_{h_1}S_{h_2}\Big(\delta_3\Big((\Upsilon_2\gamma_1{}^2 + \Upsilon_3\gamma_2\gamma_3)\delta_2 - \Upsilon_3(\gamma_1{}^2 + \gamma_2{}^2)\delta_3\Big) + \delta_1\Big(-\Big((\Upsilon_2\gamma_1 + \Upsilon_1\gamma_2)\gamma_3\delta_2\Big) + (\Upsilon_1\gamma_2{}^2 + \Upsilon_3\gamma_1\gamma_3)\delta_3\Big)\Big)\Big) + C_{h_2}(\delta_1\Big(-\Big((\Upsilon_1\gamma_1 + \Upsilon_2\gamma_2)\gamma_3\delta_2\Big) + \gamma_2(\Upsilon_1\gamma_1 + \Upsilon_3\gamma_3)\delta_3\Big) + \gamma_1\delta_2(2\Upsilon_2\gamma_3\delta_2(\Upsilon_2\gamma_2 + \Upsilon_3\gamma_3)\delta_3) + S_{h_1}S_{h_3}(\delta_1\Big(-\Big((\Upsilon_2\gamma_1\gamma_2 + \Upsilon_1\gamma_3{}^2)\delta_2\Big) + \gamma_2(\Upsilon_3\gamma_1 + \Upsilon_1\gamma_3)\delta_3\Big) + \delta_2\Big(\Upsilon_2(\gamma_1{}^2 + \gamma_3{}^2)\delta_2 - (\Upsilon_3\gamma_1{}^2 + \Upsilon_2\gamma_2\gamma_3)\delta_3))\Big) + C_{h_1}\Big(2\Upsilon_1\gamma_2\gamma_3\delta_1{}^2 - \Upsilon_1\gamma_1\gamma_3\delta_1\delta_2 - \Upsilon_2\gamma_2\gamma_3\delta_1\delta_2 - \Upsilon_1\gamma_1\gamma_2\delta_1\delta_3 - \Upsilon_3\gamma_2\gamma_3\delta_1\delta_3 + \Upsilon_2\gamma_1\gamma_2\delta_2\delta_3 + \Upsilon_3\gamma_1\gamma_3\delta_2\delta_3 + S_{h_2}S_{h3}\Big(\Upsilon_1(\gamma_2{}^2 + \gamma_3{}^2)\delta_1{}^2 + \gamma_1(\Upsilon_3\gamma_2 + \Upsilon_2\gamma_3)\delta_2\delta_3 - \delta_1(\Upsilon_1\gamma_1\gamma_2\delta_2 + \Upsilon_2\gamma_3{}^2\delta_2 + \Upsilon_3\gamma_2{}^2\delta_3 + \Upsilon_1\gamma_1\gamma_3\delta_3)\Big) - C_{h_2}C_{h_3}\Big(2\Upsilon_1\gamma_2\gamma_3\delta_1{}^2 - \delta_1\Big((\Upsilon_1\gamma_1 + \Upsilon_2\gamma_2)\gamma_3\delta_2 + +\gamma_2(\Upsilon_1\gamma_1 + \Upsilon_3\gamma_3)\delta_3\Big) + \gamma_1(2\Upsilon_2\gamma_3\delta_2{}^2 - (\Upsilon_2\gamma_2 + \Upsilon_3\gamma_3)\delta_2\delta_3 + 2\Upsilon_3\gamma_2\delta_3{}^2)\Big)\Big)\Big\} \quad \text{(A1)}$$

$$S_{qm} = \frac{Ghk}{\Delta}\{(-(\gamma_2\delta_1) + \gamma_1\delta_2)(-1 + \Upsilon_3\delta_3)((-1 + C_{h_1}C_{h_3}) \times S_{h_2}(-(\gamma_3\delta_2) + \gamma_2\delta_3) + S_{h_1}(-\gamma_3\delta_1) + S_{h_2}S_{h3}(-\gamma_2\delta_1) + \gamma_1\delta_2) + \gamma_1\delta_3 - C_{h_2}C_{h_3}(-(\gamma_3\delta_1) + \gamma_1\delta_3))) + (-1 + \Upsilon_2\delta_2)(-(\gamma_3\delta_1) + \gamma_1\delta_3)((-1 + C_{h_1}C_{h_2}) \times S_{h3}(\gamma_3\delta_2 - \gamma_2\delta_3) + S_{h_1}(-(\gamma_2\delta_1) + \gamma_1\delta_2 - C_{h_2}C_{h_3}(-(\gamma_2\delta_1) + \gamma_1\delta_2) + S_{h_2}S_{h3}(-(\gamma_3\delta_1) + \gamma_1\delta_3))) + (-1 + \Upsilon_1\delta_1)(-(\gamma_3\delta_2) + \gamma_2\delta_3)((-1 + C_{h_1}C_{h_2}) \times S_{h3}(\gamma_3\delta_1 - \gamma_1\delta_3) + S_{h_2}(\gamma_2\delta_1 - \gamma_1\delta_2 + C_{h_1}C_{h_3}(-(\gamma_2\delta_1) + \gamma_1\delta_2) + S_{h_1}S_{h3}(-(\gamma_3\delta_2) + \gamma_2\delta_3)))\} \quad \text{(A2}$$

$$S_{qt} = \frac{Ghk}{\Delta}\Big\{C_{h_3}\Big(\gamma_1\delta_2\delta_3(\Upsilon_2\delta_2 - \Upsilon_3\delta_3) + \Upsilon_1\delta_1{}^2(-(\gamma_3\delta_2) + \gamma_2\delta_3) - \delta_1\Big(\Upsilon_2\gamma_3\delta_2{}^2 - 2\Upsilon_3\gamma_3\delta_2\delta_3 + \Upsilon_3\gamma_2\delta_3{}^2\Big) - S_{h_1}S_{h_2}\Big(\gamma_3\delta_1{}^2(\Upsilon_2\delta_2 - \Upsilon_3\delta_3) + \Upsilon_3\delta_2\delta_3(-(\gamma_3\delta_2) + \gamma_2\delta_3) + \delta_1\Big(\Upsilon_1\gamma_3\delta_2{}^2 - (\Upsilon_2\gamma_1 + \Upsilon_1\gamma_2)\delta_2\delta_3 + \Upsilon_3\gamma_1\delta_3{}^2\Big)\Big)\Big) - C_{h_2}\Big(\gamma_1\delta_2\delta_3(\Upsilon_2\delta_2 - \Upsilon_3\delta_3) +$$

$$\Upsilon_1\delta_1^2(-(\gamma_3\delta_2)+\gamma_2\delta_3)+\delta_1(\Upsilon_2\gamma_3\delta_2^2-2\Upsilon_2\gamma_2\delta_2\delta_3+\Upsilon_3\gamma_2\delta_3^2)+S_{h_1}S_{h_3}(\Upsilon_2\delta_3\delta_3(\gamma_3\delta_2-\gamma_2\delta_3)+\delta_1^2(-(\Upsilon_2\gamma_2\delta_2)+\Upsilon_3\gamma_2\delta_3)+\delta_1(\Upsilon_2\gamma_1\delta_2^2-(\Upsilon_3\gamma_1+\Upsilon_1\gamma_3)\delta_2\delta_3+\Upsilon_1\gamma_2\delta_3^2)))+$$

$$C_{h_1}(-(\Upsilon_1\gamma_3\delta_1^2\delta_2)+\Upsilon_2\gamma_3\delta_1\delta_2^2-\Upsilon_1\gamma_2\delta_1^2\delta_3+2\Upsilon_1\gamma_1\delta_1\delta_2\delta_3-\Upsilon_2\gamma_1\delta_2^2\delta_3+\Upsilon_3\gamma_2\delta_1\delta_3^2-\Upsilon_3\gamma_1\delta_2\delta_3^2-S_{h_2}S_{h_3}(\gamma_1\delta_2\delta_3(\Upsilon_3\delta_2+\Upsilon_2\delta_3)+\Upsilon_1\delta_1^2(\gamma_2\delta_2+\gamma_3\delta_3)-\delta_1(\Upsilon_1\gamma_1\delta_2^2+\Upsilon_3\gamma_2\delta_2\delta_2+\Upsilon_2\gamma_3\delta_2\delta_3+\Upsilon_1\gamma_1\delta_3^2))+C_{h_3}C_{h_2}(\gamma_1\delta_2\delta_3(\Upsilon_2\delta_2+\Upsilon_3\delta_3)+\Upsilon_1\delta_1^2(\gamma_3\delta_2+\gamma_2\delta_3)+\delta_1(\Upsilon_2\gamma_3\delta_2^2-2(\Upsilon_1\gamma_1+\Upsilon_2\gamma_2+\Upsilon_3\gamma_3)\delta_2\delta_3+\Upsilon_3\gamma_2\delta_3^2)))\} \tag{A3}$$

$$S_{mm}=\frac{D}{\Delta}\{(-(\Upsilon_3\gamma_2\delta_1)+\Upsilon_2\gamma_3\delta_1+\Upsilon_3\gamma_1\delta_2-\Upsilon_1\gamma_3\delta_2-\Upsilon_2\gamma_1\delta_3+\Upsilon_1\gamma_2\delta_3)(C_{h_3}S_{h_1}S_{h_2}(-(\gamma_2\delta_1)+\gamma_1\delta_2)+S_{h_3}(C_{h_2}S_{h_1}(\gamma_3\delta_1-\gamma_1\delta_3)+C_{h_1}S_{h_2}(-(\gamma_3\delta_2)+\gamma_2\delta_3)))\} \tag{A4}$$

$$S_{mt}=\frac{D}{\Delta}\{\{(-\Upsilon_3+\alpha\nu\gamma_3)((-1+C_{h_1}C_{h_3})S_{h_2}\delta_2(-(\gamma_2\delta_1)+\gamma_1\delta_2)-(-1+C_{h_1}C_{h_2})S_{h_3}(-2\gamma_3\delta_1\delta_2+\gamma_2\delta_1\delta_3+\gamma_1\delta_2\delta_3)+S_{h_1}(C_{h_2}C_{h_3}\delta_1(\gamma_2\delta_1-\gamma_1\delta_2)+\delta_1(-(\gamma_2\delta_1)+\gamma_1\delta_2)-S_{h_2}S_{h_3}(\gamma_3\delta_1^2+\gamma_3\delta_2^2-\gamma_1\delta_1\delta_3-\gamma_2\delta_2\delta_3)))+(\Upsilon_1-\alpha\nu\gamma_1)((S_{h_2}(\delta_2-C_{h_1}C_{h_3}\delta_2)+(-1+C_{h_1}C_{h_2})S_{h_3}\delta_3)(-(\gamma_3\delta_2)+\gamma_2\delta_3)+S_{h_1}(\gamma_3\delta_1\delta_2+\gamma_2\delta_1\delta_3-2\gamma_1\delta_2\delta_3+C_{h_2}C_{h_3}(-(\gamma_3\delta_1\delta_2)-\gamma_2\delta_1\delta_3+2\gamma_1\delta_2\delta_3)-S_{h_2}S_{h_3}(-(\gamma_2\delta_1\delta_2)+\gamma_1\delta_2^2-\gamma_3\delta_1\delta_3+\gamma_1\delta_3^2)))-(\Upsilon_2-\alpha\nu\gamma_2)(((-1+C_{h_1}C_{h_2})S_{h_3}\delta_3(-(\gamma_3\delta_1)+\gamma_1\delta_3)+(-1+C_{h_1}C_{h_3})S_{h_2}(-(\gamma_3\delta_1\delta_2)+2\gamma_2\delta_1\delta_3-\gamma_1\delta_2\delta_3)+S_{h_1}(C_{h_2}C_{h_3}\delta_1(\gamma_3\delta_1-\gamma_1\delta_3)+\delta_1(-(\gamma_3\delta_1)+\gamma_1\delta_3)-S_{h_2}S_{h_3}(\gamma_2\delta_1^2-\gamma_1\delta_1\delta_2-\gamma_3\delta_2\delta_3+\gamma_2\delta_3^2)))\} \tag{A5}$$

$$S_{tt}=\frac{Gh^3}{12\Delta}\{C_{h_2}(-(\gamma_1(\Upsilon_2\gamma_2-\Upsilon_3\gamma_3)\delta_2\delta_3)-\delta_1((-(\Upsilon_1\gamma_1)+\Upsilon_2\gamma_2)\gamma_3\delta_2+\gamma_2(\Upsilon_1\gamma_1-2\Upsilon_2\gamma_2+\Upsilon_3\gamma_3)\delta_3)-S_{h_1}S_{h_3}((\Upsilon_2\gamma_2-\Upsilon_3\gamma_3)\delta_1(-(\gamma_2\delta_1)+\gamma_1\delta_2)+(-(\Upsilon_1\gamma_1)+\Upsilon_2\gamma_2)\gamma_3\delta_2\delta_3+\gamma_2(\Upsilon_1\gamma_1-\Upsilon_2\gamma_2)\delta_3^2))-C_{h_3}(\gamma_1(-(\Upsilon_2\gamma_2)+\Upsilon_3\gamma_3)\delta_2\delta_3+\delta_1(\Upsilon_1\gamma_1+\Upsilon_2\gamma_2-2\Upsilon_3\gamma_3)\delta_2+(-(\Upsilon_1\gamma_1\gamma_2)+\Upsilon_3\gamma_2\gamma_3)\delta_3)+S_{h_1}S_{h_2}(\gamma_3(\Upsilon_1\gamma_1-\Upsilon_3\gamma_3)\delta_2^2+\gamma_2(-(\Upsilon_1\gamma_1)+\Upsilon_3\gamma_3)\delta_2\delta_3+(-(\Upsilon_2\gamma_2)+\Upsilon_3\gamma_3)\delta_1(-(\gamma_3\delta_1)+\gamma_1\delta_3)))+C_{h_1}(-(\Upsilon_1\gamma_1\gamma_3\delta_1\delta_2)+\Upsilon_2\gamma_2\gamma_3\delta_1\delta_2-\Upsilon_1\gamma_1\gamma_2\delta_1\delta_3+\Upsilon_3\gamma_2\gamma_3\delta_1\delta_3+2\Upsilon_1\gamma_1^2\delta_2\delta_3-\Upsilon_2\gamma_1\gamma_2\delta_2\delta_3-\Upsilon_3\gamma_1\gamma_3\delta_2\delta_3+$$

$$S_{h_2}S_{h_3}\Big(\gamma_2(-(\Upsilon_1\gamma_1)+\Upsilon_3\gamma_3)\delta_1\delta_2+\gamma_1(\Upsilon_1\gamma_1-\Upsilon_3\gamma_3)\delta_2{}^2+(\Upsilon_1\gamma_1-\Upsilon_2\gamma_2)\delta_3(-(\gamma_3\delta_1)+\gamma_1\delta_3)\Big)-C_{h_2}C_{h_3}(\gamma_2(-(\Upsilon_1\gamma_1)+2\Upsilon_2\gamma_2-\Upsilon_3\gamma_3)\delta_1\delta_3+\delta_2(\gamma_3(-(\Upsilon_1\gamma_1)-\Upsilon_2\gamma_2+2\Upsilon_3\gamma_3)\delta_1+\gamma_1(2\Upsilon_1\gamma_1-\Upsilon_2\gamma_2-\Upsilon_3\gamma_3)\delta_3)))\Big\} \tag{A6}$$

$$f_{mm}=\frac{D}{\Delta}\{-(\Upsilon_3\gamma_2\delta_1)+\Upsilon_2\gamma_3\delta_1+\Upsilon_3\gamma_1\delta_2-\Upsilon_1\gamma_3\delta_2-\Upsilon_2\gamma_1\delta_3+\Upsilon_1\gamma_2\delta_3)(S_{h_2}S_{h_3}(\gamma_3\delta_2-\gamma_2\delta_3)+S_{h_1}(S_{h_2}(\gamma_2\delta_1-\gamma_1\delta_2)+S_{h_3}(-(\gamma_3\delta_1)+\gamma_1\delta_3))\} \tag{A7}$$

$$f_{mt}=-\frac{D}{\Delta}\{\Upsilon_3\gamma_2\delta_1-\Upsilon_2\gamma_3\delta_1-\Upsilon_3\gamma_1\delta_2+\Upsilon_1\gamma_3\delta_2+\Upsilon_2\gamma_1\delta_3-\Upsilon_1\gamma_2\delta_3)(C_{h_3}(-(S_{h_1}\delta_1)+S_{h_2}\delta_2)+C_{h_2}(S_{h_1}\delta_1-S_{h_3}\delta_3)+C_{h_1}(-(S_{h_2}\delta_2)+S_{h_3}\delta_3)\} \tag{A8}$$

$$f_{qm}=\frac{Ghk}{\Delta}\Big\{-\Big(C_{h_1}(-(\gamma_3\delta_2)+\gamma_2\delta_3)\Big(S_{h_2}(-(\gamma_2\delta_1)+\gamma_1\delta_2)(\Upsilon_1\delta_1-\Upsilon_3\delta_3)+S_{h_3}(\Upsilon_1\delta_1-\Upsilon_2\delta_2)(\gamma_3\delta_1-\gamma_1\delta_3)\Big)\Big)+C_{h_2}(-(\gamma_3\delta_1)+\gamma_1\delta_3)(S_{h_1}(-(\gamma_2\delta_1)+\gamma_1\delta_2)(\Upsilon_2\delta_2-\Upsilon_3\delta_3)+S_{h_3}(-(\Upsilon_1\delta_1+\Upsilon_2\delta_2)(-(\gamma_3\delta_2)+\gamma_2\delta_3))+C_{h_3}(-(\gamma_2\delta_1)+\gamma_1\delta_2)(S_{h_1}(-(\Upsilon_2\delta_2)+\Upsilon_3\delta_3)(-(\gamma_3\delta_1)+\gamma_1\delta_3)+S_{h_2}(\Upsilon_1\delta_1-\Upsilon_3\delta_3)(-(\gamma_3\delta_2)+\gamma_2\delta_3))\Big\} \tag{A9}$$

$$f_{qq}=\frac{Ghk}{\Delta}\Big\{-(\Upsilon_1S_{h_2}S_{h_3}\gamma_2{}^2\delta_1{}^2)-2\Upsilon_1\gamma_2\gamma_3\delta_1{}^2-\Upsilon_1S_{h_2}S_{h_3}\gamma_3{}^2\delta_1{}^2+\Upsilon_2S_{h_1}S_{h_3}\gamma_1\gamma_2\delta_1\delta_2+\Upsilon_1S_{h_2}S_{h_3}\gamma_1\gamma_2\delta_1\delta_2+\Upsilon_1\gamma_1\gamma_3\delta_1\delta_2-\Upsilon_2S_{h_1}S_{h_2}\gamma_1\gamma_3\delta_1\delta_2+\Upsilon_2\gamma_2\gamma_3\delta_1\delta_2-\Upsilon_1S_{h_1}S_{h_2}\gamma_2\gamma_3\delta_1\delta_2+\Upsilon_1S_{h_1}S_{h_2}\gamma_3{}^2\delta_1\delta_2+\Upsilon_2S_{h_2}S_{h_3}\gamma_3{}^2\delta_1\delta_2-\Upsilon_2S_{h_1}S_{h_3}\gamma_1{}^2\delta_2{}^2-2\Upsilon_2\gamma_1\gamma_3\delta_2{}^2-\Upsilon_2S_{h_1}S_{h_3}\gamma_3{}^2\delta_2{}^2+\Upsilon_1\gamma_1\gamma_2\delta_1\delta_3-\Upsilon_3S_{h_1}S_{h_3}\gamma_1\gamma_2\delta_1\delta_3+\Upsilon_1S_{h_1}S_{h_2}\gamma_2{}^2\delta_1\delta_3+\Upsilon_3S_{h_2}S_{h_3}\gamma_2{}^2\delta_1\delta_3+\Upsilon_3S_{h_1}S_{h_2}\gamma_1\gamma_3\delta_1\delta_3+\Upsilon_1S_{h_2}S_{h_3}\gamma_1\gamma_3\delta_1\delta_3+\Upsilon_3\gamma_2\gamma_3\delta_1\delta_3-\Upsilon_1S_{h_1}S_{h_3}\gamma_2\gamma_3\delta_1\delta_3+\Upsilon_2S_{h_1}S_{h_2}\gamma_1{}^2\delta_2\delta_3+\Upsilon_3S_{h_1}S_{h_3}\gamma_1{}^2\delta_2\delta_3+\Upsilon_2\gamma_1\gamma_2\delta_2\delta_3-\Upsilon_3S_{h_2}S_{h_3}\gamma_1\gamma_2\delta_2\delta_3+\Upsilon_3\gamma_1\gamma_3\delta_2\delta_3-\Upsilon_2S_{h_2}S_{h_3}\gamma_1\gamma_3\delta_2\delta_3+\Upsilon_3S_{h_1}S_{h_2}\gamma_2\gamma_3\delta_2\delta_3+\Upsilon_2S_{h_1}S_{h_3}\gamma_2\gamma_3\delta_2\delta_3-\Upsilon_3S_{h_1}S_{h_2}\gamma_1{}^2\delta_3{}^2-2\Upsilon_3\gamma_1\gamma_2\delta_3{}^2-\Upsilon_3S_{h_1}S_{h_2}\gamma_2{}^2\delta_3{}^2+C_{h_2}C_{h_3}\Big(2\Upsilon_1\gamma_2\gamma_3\delta_1{}^2+\gamma_1(\Upsilon_2\gamma_2+\Upsilon_3\gamma_3)\delta_2\delta_3-\delta_1(\Upsilon_1\gamma_1\gamma_3\delta_2+\Upsilon_2\gamma_2\gamma_3\delta_2+\Upsilon_1\gamma_1\gamma_2\delta_3+\Upsilon_3\gamma_2\gamma_3\delta_3)\Big)-C_{h_1}(C_{h_3}\Big(\gamma_1\delta_2(-2\Upsilon_2\gamma_3\delta_2+\Upsilon_2\gamma_2\delta_3+\Upsilon_3\gamma_3\delta_3)+\delta_1\big((\Upsilon_1\gamma_1+\Upsilon_2\gamma_2)\gamma_3\delta_2-\gamma_2(\Upsilon_1\gamma_1+\Upsilon_3\gamma_3)\delta_3\big)\Big)+C_{h_2}\Big(\gamma_1\delta_3(\Upsilon_2\gamma_2\delta_2+\Upsilon_3\gamma_3\delta_2-2\Upsilon_3\gamma_2\delta_3)+\delta_1\big(-((\Upsilon_1\gamma_1+\Upsilon_2\gamma_2)\gamma_3\delta_2)+\gamma_2(\Upsilon_1\gamma_1+\Upsilon_3\gamma_3)\delta_3\big)\Big)\Big\} \tag{A10}$$

$$f_{qt}=\frac{Ghk}{\Delta}\Big\{-(\Upsilon_2S_{h_1}S_{h_3}\gamma_2\delta_1{}^2\delta_2)+\Upsilon_1S_{h_2}S_{h_3}\gamma_2\delta_1{}^2\delta_2+\Upsilon_1\gamma_3\delta_1{}^2\delta_2+\Upsilon_2S_{h_1}S_{h_2}\gamma_3\delta_1{}^2\delta_2+\Upsilon_2S_{h_1}S_{h_3}\gamma_1\delta_1\delta_2{}^2-\Upsilon_1S_{h_2}S_{h_3}\gamma_1\delta_2\delta_2{}^2+\Upsilon_2\gamma_3\delta_1\delta_2{}^2+\Upsilon_1S_{h_1}S_{h_2}\gamma_3\delta_1\delta_2{}^2+\Upsilon_1\gamma_2\delta_1{}^2\delta_3+$$

$$\Upsilon_3 S_{h_1} S_{h_3} \gamma_2 {\delta_1}^2 \delta_3 - \Upsilon_3 S_{h_1} S_{h_2} \gamma_3 {\delta_1}^2 \delta_3 + \Upsilon_1 S_{h_2} S_{h_3} \gamma_3 {\delta_1}^2 \delta_3 - 2\Upsilon_1 \gamma_1 \delta_1 \delta_2 \delta_3 -$$
$$\Upsilon_2 S_{h_1} S_{h_2} \gamma_1 \delta_1 \delta_2 \delta_3 - \Upsilon_3 S_{h_1} S_{h_3} \gamma_1 \delta_1 \delta_2 \delta_3 - 2\Upsilon_2 \gamma_2 \delta_1 \delta_2 \delta_3 - \Upsilon_1 S_{h_1} S_{h_2} \gamma_2 \delta_1 \delta_2 \delta_3 -$$
$$\Upsilon_3 S_{h_2} S_{h_3} \gamma_2 \delta_1 \delta_2 \delta_3 - 2\Upsilon_3 \gamma_3 \delta_1 \delta_2 \delta_3 - \Upsilon_1 S_{h_1} S_{h_3} \gamma_3 \delta_1 \delta_2 \delta_3 - \Upsilon_2 S_{h_2} S_{h_3} \gamma_3 \delta_1 \delta_2 \delta_3 +$$
$$\Upsilon_2 \gamma_1 {\delta_2}^2 \delta_3 + \Upsilon_3 S_{h_2} S_{h_3} \gamma_1 {\delta_2}^2 \delta_3 - \Upsilon_3 S_{h_1} S_{h_2} \gamma_3 {\delta_2}^2 \delta_3 + \Upsilon_2 S_{h_1} S_{h_3} \gamma_3 {\delta_2}^2 \delta_3 +$$
$$\Upsilon_3 S_{h_1} S_{h_2} \gamma_1 \delta_1 {\delta_3}^2 - \Upsilon_1 S_{h_2} S_{h_3} \gamma_1 \delta_1 {\delta_3}^2 + \Upsilon_3 \gamma_2 \delta_1 {\delta_3}^2 + \Upsilon_1 S_{h_1} S_{h_3} \gamma_2 \delta_1 {\delta_3}^2 + \Upsilon_3 \gamma_1 \delta_2 {\delta_3}^2 +$$
$$\Upsilon_2 S_{h_2} S_{h_3} \gamma_1 \delta_2 {\delta_3}^2 + \Upsilon_3 S_{h_1} S_{h_2} \gamma_2 \delta_2 {\delta_3}^2 - \Upsilon_2 S_{h_1} S_{h_3} \gamma_2 \delta_2 {\delta_3}^2 - C_{h_2} C_{h_3} \Big(\gamma_1 \delta_2 \delta_3 (\Upsilon_2 \delta_2 +$$
$$\Upsilon_3 \delta_3) + \Upsilon_1 {\delta_1}^2 (\gamma_3 \delta_2 + \gamma_2 \delta_3) - \delta_1 (\Upsilon_2 \gamma_3 {\delta_2}^2 + 2\Upsilon_1 \gamma_1 \delta_2 \delta_3 + \Upsilon_3 \gamma_2 {\delta_3}^2) \Big) +$$
$$C_{h_1} (- \Big(C_{h_3} \Big(\gamma_1 \delta_2 \delta_3 (\Upsilon_2 \delta_2 - \Upsilon_3 \delta_3) + \Upsilon_1 {\delta_1}^2 (-(\gamma_3 \delta_2) + \gamma_2 \delta_3) + \delta_1 (\Upsilon_2 \gamma_3 {\delta_2}^2 - 2\Upsilon_2 \gamma_2 \delta_2 \delta_3 +$$
$$\Upsilon_3 \gamma_2 {\delta_3}^2) \Big) \Big) + C_{h_2} (\gamma_1 \delta_2 \delta_3 (\Upsilon_2 \delta_2 - \Upsilon_3 \delta_3) + \Upsilon_1 {\delta_1}^2 \Big(-(\gamma_3 \delta_2) + \gamma_2 \delta_3) - \delta_1 (\Upsilon_2 \gamma_3 {\delta_2}^2 -$$
$$2\Upsilon_3 \gamma_3 \delta_2 \delta_3 + \Upsilon_3 \gamma_2 {\delta_3}^2))) \Big) \Big\} \qquad \text{(A11)}$$

$$f_{tt} = \frac{Gh3}{12\Delta} \Big\{ -(\Upsilon_2 S_{h_1} S_{h_3} {\gamma_2}^2 {\delta_1}^2) + \Upsilon_2 S_{h_1} S_{h_2} \gamma_2 \gamma_3 {\delta_1}^2 + \Upsilon_3 S_{h_1} S_{h_3} \gamma_2 \gamma_3 {\delta_1}^2 - \Upsilon_3 S_{h_1} S_{h_2} {\gamma_3}^2 {\delta_1}^2 +$$
$$\Upsilon_2 S_{h_1} S_{h_3} \gamma_1 \gamma_2 \delta_1 \delta_2 + \Upsilon_1 S_{h_2} S_{h_3} \gamma_1 \gamma_2 \delta_1 \delta_2 + \Upsilon_1 \gamma_1 \gamma_3 \delta_1 \delta_2 - \Upsilon_3 S_{h_1} S_{h_3} \gamma_1 \gamma_3 \delta_1 \delta_2 +$$
$$\Upsilon_2 \gamma_2 \gamma_3 \delta_1 \delta_2 - \Upsilon_3 S_{h_2} S_{h_3} \gamma_2 \gamma_3 \delta_1 \delta_2 - 2\Upsilon_3 {\gamma_3}^2 \delta_1 \delta_2 - \Upsilon_1 S_{h_2} S_{h_3} {\gamma_1}^2 {\delta_2}^2 + \Upsilon_1 S_{h_1} S_{h_2} \gamma_1 \gamma_3 {\delta_2}^2 +$$
$$\Upsilon_3 S_{h_2} S_{h_3} \gamma_1 \gamma_3 {\delta_2}^2 - \Upsilon_3 S_{h_1} S_{h_2} {\gamma_3}^2 {\delta_2}^2 + \Upsilon_1 \gamma_1 \gamma_2 \delta_1 \delta_3 - \Upsilon_2 S_{h_1} S_{h_2} \gamma_1 \gamma_2 \delta_1 \delta_3 - 2\Upsilon_2 {\gamma_2}^2 \delta_1 \delta_3 +$$
$$\Upsilon_3 S_{h_1} S_{h_2} \gamma_1 \gamma_3 \delta_1 \delta_3 + \Upsilon_1 S_{h_2} S_{h_3} \gamma_1 \gamma_3 \delta_1 \delta_3 + \Upsilon_3 \gamma_2 \gamma_3 \delta_1 \delta_3 - \Upsilon_2 S_{h_2} S_{h_3} \gamma_2 \gamma_3 \delta_1 \delta_3 -$$
$$2\Upsilon_1 {\gamma_1}^2 \delta_2 \delta_3 + \Upsilon_2 \gamma_1 \gamma_2 \delta_2 \delta_3 - \Upsilon_1 S_{h_1} S_{h_2} \gamma_1 \gamma_2 \delta_2 \delta_3 + \Upsilon_3 \gamma_1 \gamma_3 \delta_2 \delta_3 - \Upsilon_1 S_{h_1} S_{h_3} \gamma_1 \gamma_3 \delta_2 \delta_3 +$$
$$\Upsilon_3 S_{h_1} S_{h_2} \gamma_2 \gamma_3 \delta_2 \delta_3 + \Upsilon_2 S_{h_1} S_{h_3} \gamma_2 \gamma_3 \delta_2 \delta_3 - \Upsilon_1 S_{h_2} S_{h_3} {\gamma_1}^2 {\delta_3}^2 + \Upsilon_1 S_{h_1} S_{h_3} \gamma_1 \gamma_2 {\delta_3}^2 +$$
$$\Upsilon_2 S_{h_2} S_{h_3} \gamma_1 \gamma_2 {\delta_3}^2 - \Upsilon_2 S_{h_1} S_{h_3} {\gamma_2}^2 {\delta_3}^2 + C_{h_2} C_{h_3} \Big(\gamma_2 (-(\Upsilon_1 \gamma_1) + \Upsilon_3 \gamma_3) \delta_1 \delta_3 +$$
$$\delta_2 ((-(\Upsilon_1 \gamma_1) + \Upsilon_2 \gamma_2) \gamma_3 \delta_1 + \gamma_1 (2\Upsilon_1 \gamma_1 - \Upsilon_2 \gamma_2 - \Upsilon_3 \gamma_3) \delta_3) \Big) + C_{h_1} (C_{h_2} (\gamma_1 (\Upsilon_2 \gamma_2 -$$
$$\Upsilon_3 \gamma_3) \delta_2 \delta_3 + \delta_1 (\gamma_3 (-(\Upsilon_1 \gamma_1) - \Upsilon_2 \gamma_2 + 2\Upsilon_3 \gamma_3) \delta_2 + \gamma_2 (\Upsilon_1 \gamma_1 - \Upsilon_3 \gamma_3) \delta_3)) -$$
$$C_{h_3} \Big(\gamma_1 (\Upsilon_2 \gamma_2 - \Upsilon_3 \gamma_3) \delta_2 \delta_3 + \delta_1 ((-(\Upsilon_1 \gamma_1) + \Upsilon_2 \gamma_2) \gamma_3 \delta_2 + \gamma_2 (\Upsilon_1 \gamma_1 - 2\Upsilon_2 \gamma_2 + \Upsilon_3 \gamma_3) \delta_3)) \Big) \Big\}$$

(A12)

$$\Delta = -2 \Big\{ (-(\gamma_3 \delta_2) + \gamma_2 \delta_3) \Big((-1 + C_{h_1} C_{h_3}) S_{h_2} (\gamma_2 \delta_1 - \gamma_1 \delta_2) + (-1 +$$
$$C_{h_1} C_{h_2}) S_{h_3} (-(\gamma_3 \delta_1) + \gamma_1 \delta_3) \Big) + + S_{h_1} (2(-(\gamma_2 \delta_1) + \gamma_1 \delta_2)(-(\gamma_3 \delta_1) + \gamma_1 \delta_3) -$$
$$2 C_{h_2} C_{h_3} (-(\gamma_2 \delta_1) + \gamma_1 \delta_2)(-(\gamma_3 \delta_1) + \gamma_1 \delta_3) + S_{h_2} S_{h_3} \Big(({\gamma_2}^2 + {\gamma_3}^2) {\delta_1}^2 + ({\gamma_1}^2 + {\gamma_3}^2) +$$
$${\delta_2}^2 - 2\gamma_1 \gamma_3 \delta_1 \delta_3 + ({\gamma_1}^2 + {\gamma_2}^2) {\delta_3}^2 - 2\gamma_2 \delta_2 (\gamma_1 \delta_1 + \gamma_3 \delta_3)) \Big) \Big\} \qquad \text{(A13)}$$

References

[1] Reddy JN. Analysis of functionally graded plates.Int J Numer Methods Eng 2000;47(1-3):663-684 https://doi.org/10.1002/(SICI)10970207(20000110/30)47:1/3<663:AID-NME787>3.0.CO;2-8.

[2] Hasselman DP, Youngblood GE. Enhanced thermal stress resistance of structural ceramics with thermal conductivity gradient. J Am Ceramic Soc 1978; 61(1-2):49-52.

[3] Zhang N, Khan T, Guo H, Shi S, Zhong W, Zhang W. Functionally Graded Materials: An Overview of Stability, Buckling, and Free Vibration Analysis. Adv Mater Sci Eng 2019;2019(1):13541501-18. https://doi.org/10.1155/2019/1354150.

[4] Chung, Yen-Ling, Chi SH. The residual stress of functionally graded materials. J Chinese Inst Civ Hydraul Eng 2001;13:1–9.

[5] Lee WY, Stinton DP, Berndt CC, Erdogan F, Lee Y Der, Mutasim Z. Concept of functionally graded materials for advanced thermal barrier coating applications. J Am Ceram Soc 1996;79:3003–12. https://doi.org/10.1111/j.1151-2916.1996.tb08070.x.

[6] Jin ZH, Batra RC. Stress intensity relaxation at the tip of an edge crack in a functionally graded material subjected to a thermal shock. J Therm Stress 1996;19(4):317-339. https://doi.org/10.1080/01495739608946178.

[7] Delale F, Erdogan F. The crack problem for a nonhomogeneous plane. J Appl Mech Trans ASME 1983;50(3):609-614. https://doi.org/10.1115/1.3167098.

[8] Gu P, Asaro RJ. Crack deflection in functionally graded materials. Int J Solids Struct 1997;34(24):3085-3098. https://doi.org/10.1016/S0020-7683(96)00175-8.

[9] Erdogan F, Wu BH. Crack problems in FGM layers under thermal stresses. J Therm Stress 1996;19(3):237-265. https://doi.org/10.1080/01495739608946172.

[10] Jin ZH, Noda N. Crack-tip singular fields in nonhomogeneous materials. J Appl Mech Trans ASME 1994;61(3):738-740. https://doi.org/10.1115/1.2901529.

[11] Erdogan YF, Chen F. Interfacial cracking of FGM metal bonds. In: Kokini K, editor, Ceramic Coating. 1998: 29–37.

[12]] Ali MI, Azam MS, Ranjan V, Banerjee JR. Free vibration of sigmoid functionally graded plates using the dynamic stiffness method and the Wittrick-Williams algorithm. Comput Struct 2021;244:1064241-17.

[13] Chi SH, Chung Y-L. Cracking in sigmoid functionally graded coating. J Mech 2002; 18:41–53.

[14] Zhang DG. Modeling and analysis of FGM rectangular plates based on physical neutral surface and high order shear deformation theory. Int J Mech Sci 2013;68:92–104. https://doi.org/10.1016/j.ijmecsci.2013.01.002.

[15] Zhang DG, Zhou YH. A theoretical analysis of FGM thin plates based on physical neutral surface. Comput Mater Sci 2008;44:716–20. https://doi.org/10.1016/j.commatsci.2008.05.016.

[16] Yin S, Yu T, Liu P. Free vibration analyses of FGM thin plates by isogeometric analysis based on classical plate theory and physical neutral surface. Adv Mech Eng 2013;5: 6345841-10. https://doi.org/10.1155/2013/634584.

[17] Kim N Il, Lee J. Geometrically nonlinear isogeometric analysis of functionally graded plates based on first-order shear deformation theory considering physical neutral surface. Compos Struct 2016;153:804–814. https://doi.org/10.1016/j.compstruct.2016.07.002.

[18] Lee YH, Bae SI, Kim JH. Thermal buckling behavior of functionally graded plates based on neutral surface. Compos Struct 2016;137:208–214. https://doi.org/10.1016/j.compstruct.2015.11.023.

[19] Zhang DG. Nonlinear bending analysis of FGM beams based on physical neutral surface and high order shear deformation theory. Compos Struct 2013; 100:121–126. https://doi.org/10.1016/j.compstruct.2012.12.024.

[20] Benadouda M, El Amin Bourouis M, Dahmane M, Bennai R, Atmane, HA, Safer O. Dynamic response of wave propagation in functionally graded beams with defects: effects of porosity and cracks. Acta Mechanica ;236: 2279-2296

[21] Lakel A, Hadji L, Avcar M, Atmane HA, Madan R. The natural frequency analysis of FG-GNPR nanoplates under different boundary conditions. Adv nano research 2024; 17(6):533-546.

[22] Ghalem M, Zahaf S, Dahmane M, Atmane HA, Bennai R. Natural frequencies of 2D-FG beams with internal crack defects on Winkler–Pasternak elastic foundation using finite element technique. Mech Based Des Struct Mach 2025; 1-18. https://doi.org/10.1080/15397734.2025.2458097

[23] Khayra D, Meziane MAA, Hadji L, Atmane HA, Bennai R, Madan R. Effect of porosity and boundary conditions on dynamic characteristics of cracked plates made of functionally graded materials. Adv concrete const 2024; 18(3): 175-190.

[24] Doori SGM, Noori AR, Etemadi A. Static Response of Functionally Graded Porous Circular Plates via Finite Element Method. Arab J Sci Engg 2024; 49(10): 14167–14181. https://doi.org/10.1007/s13369-024-08914-w

[25] Banerjee JR. Dynamic stiffness formulation for structural elements: A general approach. Comput Struct 1997;63(1):101–103. https://doi.org/10.1016/S0045-7949(96)00326-4.

[26] Banerjee JR, Williams FW. Coupled bending-torsional dynamic stiffness matrix for timoshenko beam elements. Comput Struct 1992;42(3):301-310. https://doi.org/10.1016/0045-7949(92)90026-V.

[27] Banerjee JR. Free vibration analysis of a twisted beam using the dynamic stiffness method. Int J Solids Struct 2001; 38(38-39): 6703-6722. https://doi.org/10.1016/S0020-7683(01)00119-6.

[28] Banerjee JR. Free vibration of sandwich beams using the dynamic stiffness method. Comput Struct 2003;81(18-19):1915-1922.https://doi.org/10.1016/S0045-7949(03)00211-6.

[29] Banerjee JR. Development of an exact dynamic stiffness matrix for free vibration analysis of a twisted Timoshenko beam. J Sound Vib 2004;270(1-2):379-401 https://doi.org/10.1016/S0022-460X(03)00633-3.

[30] Banerjee JR, Su H, Jackson DR. Free vibration of rotating tapered beams using the dynamic stiffness method. J Sound Vib 2006;298(4-5):1034-1054 https://doi.org/10.1016/j.jsv.2006.06.040.

[31] Banerjee JR, Cheung CW, Morishima R, Perera M, Njuguna J. Free vibration of a three-layered sandwich beam using the dynamic stiffness method and experiment. Int J Solids Struct 2007;44(22-23):7543-7563 https://doi.org/10.1016/j.ijsolstr.2007.04.024.

[32] Boscolo M, Banerjee JR. Dynamic stiffness elements and their applications for plates using first order shear deformation theory. Comput Struct 2011; 89: 395–410. https://doi.org/10.1016/j.compstruc.2010.11.005.

[33] Boscolo M, Banerjee JR. Dynamic stiffness method for exact inplane free vibration analysis of plates and plate assemblies. J Sound Vib 2011;330(12): 2928-2936. doi:10.1016/j.jsv.2010.12.022.

[34] Papkov S, Banerjee JR. A new method for free vibration and buckling analysis of rectangular orthotropic plates. 2015; 339: 342-358. doi:10.1016/j.jsv.2014.11.007.

[35] Banerjee JR, Papkov SO, Liu X, Kennedy D. Dynamic stiffness matrix of a rectangular plate for the general case. J Sound Vib 2015;342:177–199. doi:https://doi.org/10.1016/j.jsv.2014.12.031.

[36] Liu X, Banerjee JR. Free vibration analysis for plates with arbitrary boundary conditions using a novel spectral-dynamic stiffness method. Comput Struct 2016;164:108–126. doi:https://doi.org/10.1016/j.compstruc.2015.11.005.

[37] Ghorbel O, Casimir JB, Hammami L, Tawfiq I, Haddar M. Dynamic stiffness formulation for free orthotropic plates. J Sound Vib 2015;346:361–375. doi:https://doi.org/10.1016/j.jsv.2015.02.020.

[38] Ghorbel O, Casimir JB, Hammami L, Tawfiq I, Haddar M. In-plane dynamic stiffness matrix for a free orthotropic plate. J Sound Vib 2016;364:234–246. doi:https://doi.org/10.1016/j.jsv.2015.11.028.

[39] Boscolo M, Banerjee JR. Dynamic stiffness formulation for composite Mindlin plates for exact modal analysis of structures. Part I: Theory. Comput Struct 2012;96–97:74–83. doi:10.1016/j.compstruc.2012.01.002.

[40] Boscolo M, Banerjee JR. Dynamic stiffness formulation for composite Mindlin plates for exact modal analysis of structures. Part II: Results and applications. Comput Struct 2012;96–97: 74–83. doi:https://doi.org/10.1016/j.compstruc.2012.01.003.

[41] Boscolo M, Banerjee JR. Layer-wise dynamic stiffness solution for free vibration analysis of laminated composite plates. J Sound Vib 2014;333:200–227. doi:10.1016/j.jsv.2013.08.031.

[42] Liu X, Banerjee JR. An exact spectral-dynamic stiffness method for free flexural vibration analysis of orthotropic composite plate assemblies – Part I: Theory. Compos Struct 2015;132:1274–1287. doi:https://doi.org/10.1016/j.compstruct.2015.07.020.

[43] Liu X, Banerjee JR. An exact spectral-dynamic stiffness method for free flexural vibration analysis of orthotropic composite plate assemblies – Part II: Applications. Compos Struct 2015;132:1288–1302. doi:https://doi.org/10.1016/j.compstruct.2015.07.022.

[44] Fazzolari FA, Boscolo M, Banerjee JR. An exact dynamic stiffness element using a higher order shear deformation theory for free vibration analysis of composite plate assemblies. Compos Struct 2013;96:262–278. doi:10.1016/j.compstruct.2012.08.033.

[45] Thinh TI, Nguyen MC, Ninh DG. Dynamic stiffness formulation for vibration analysis of thick composite plates resting on non-homogenous foundations. Compos Struct 2014; 108:684–695. doi:10.1016/j.compstruct.2013.10.022.

[46] Pagani A, Carrera E, Boscolo M, Banerjee JR. Refined dynamic stiffness elements applied to free vibration analysis of generally laminated composite beams with arbitrary boundary conditions. Compos Struct 2014;110:305–316. doi:10.1016/j.compstruct.2013.12.010.

[47] Kolarevic N, Marjanović M, Nefovska-Danilovic M, Petronijevic M. Free vibration analysis of plate assemblies using the dynamic stiffness method based on the higher order shear deformation theory. J Sound Vib 2016;364:110–132. doi:10.1016/j.jsv.2015.11.016.

[48] Leissa AW. The free vibration of rectangular plates. J Sound Vib 1973;31(3):257-293.

[49] Chakraverty S, Pradhan KK. Free vibration of exponential functionally graded rectangular plates in thermal environment with general boundary conditions. Aerospace Sci Tech 2014;36:132-156.

[50] Abrate S. Functionally graded plates behave like homogeneous plates. Compos part B: engg 2008;39(1):151-158.

[51] Reissner E. The effect of transverse shear deformation on the bending of elastic plates. J Appl Mechanics 1945;12(2):69-77

[52] Mindlin RD. Influence of rotatory inertia and shear on flexural motions of isotropic, elastic plates. J Appl Mechanics 1951;18:31-38

[53] Thai HT, Nguyen TK, Vo TP, Lee J. Analysis of functionally graded sandwich plates using a new first-order shear deformation theory. European J Mechanics-A/Solids 2014;

45:211-225.

[54] Meksi A, Benyoucef S, Houari MS, Tounsi A. A simple shear deformation theory based on neutral surface position for functionally graded plates resting on Pasternak elastic foundations. Struct engg mechanics: An int J 2015;53(6):1215-1240.

[55] Hosseini-Hashemi S, Fadaee MO, Atashipour SR. A new exact analytical approach for free vibration of Reissner–Mindlin functionally graded rectangular plates. Int J Mech Sci 2011;53(1):11-22.

[56] Thai HT, Choi DH. A simple first-order shear deformation theory for the bending and free vibration analysis of functionally graded plates. Compos Struct 2013;101:332-340

[57] Hosseini-Hashemi S, Taher HR, Akhavan H, Omidi M. Free vibration of functionally graded rectangular plates using first-order shear deformation plate theory. Appl Math Model. 2010;34(5):1276-1291.

[58] Li H, Liu N, Pang F, Du Y, Li S. An accurate solution method for the static and vibration analysis of functionally graded Reissner-Mindlin rectangular plate with general boundary conditions. Shock Vib 2018;2018(1):4535871-21.https://doi.org/10.1155/2018/4535871

[59] Bellifa H, Benrahou KH, Hadji L, Houari MS, Tounsi A. Bending and free vibration analysis of functionally graded plates using a simple shear deformation theory and the concept the neutral surface position. J Brazilian Society Mech Sci Engg 2016; 38(1):265-75.

[60] Fallah A, Aghdam MM, Kargarnovin MH. Free vibration analysis of moderately thick functionally graded plates on elastic foundation using the extended Kantorovich method. Arch Appl Mechanics 2013; 83(2):177-91.

[61] Yin S, Hale JS, Yu T, Bui TQ, Bordas SP. Isogeometric locking-free plate element: a simple first order shear deformation theory for functionally graded plates. Compos Struct 2014;118:121-138.

[62] Nebab M, Dahmane M, Atmane HA, Bernard F, Benadouda M, Bennai R, Hadji L. Fundamental frequencies of cracked FGM beams with influence of porosity and Winkler/Pasternak/Kerr foundation support using a new quasi-3D HSDT. Mech Adv Mater Struct 2024; 31(28): 10639–10651.

[63] Atmane RA, Mahmoudi N, Bennai R, Atmane HA, Tounsi A**.** Investigation on the dynamic response of porous FGM beams resting on variable foundation using a new higher order shear deformation theory. Steel Compos Struct 2021; 39(1): 95–107. https://doi.org/10.12989/scs.2021.39.1.095

[64] Zouatnia N, Hadji L, Atmane HA, Nebab, M, Madan R, Bennai R, Dahmane M. Analysis of free vibration in bi-directional power law-based FG beams employing RSD theory. Coupled Systems Mechanics 2024; 13(4): 359-373.

[65] Hadji L, Plevris V, Madan R, Atmane HA. Multi-directional functionally graded sandwich plates: buckling and free vibration analysis with refined plate models under various boundary conditions. Computation 2024; 12(4): 651-20.

[66] Hadji L, Madan R, Atmane HA, Bernard F, Zouatnia N, Safa A.Thermal buckling analysis of functionally graded plates using trigonometric shear deformation theory for temperature-dependent material properties. Struct Engg Mechanics 2024; 91(6): 539-549.

[67] Debbaghi S, Dahmane M, Benadouda M, Atmane HA, Bendenia N, Hadji L.Wave propagation of bi-directional porous FG beams using Touratier's higher-order shear deformation beam theory. Coupl sys mechanics 2024; 13(1): 43-60.

[68] Bennai R, Atmane HA, Tounsi A. A new higher-order shear and normal deformation theory for functionally graded sandwich beams. Steel Compos Struct 2015;19(3): 521-546.

[69] Dahmane M, Benadouda M, Fellah A, Saimi A, Hassen AA, Bensaid I. Porosities-dependent wave propagation in bi-directional functionally graded cantilever beam with higher-order shear model. Mech Adv Mater Struct 2024; 31(26): 8018-8028.

[70] Mellal F, Bennai R, Avcar M, Nebab M, Atmane HA.On the vibration and buckling behaviors of porous FG beams resting on variable elastic foundation utilizing higher-order shear deformation theory. Acta Mechanica 2023; 234(9): 3955-3977.

[71] Bennai R, Atmane RA, Bernard F, Nebab M, Mahmoudi N, Atmane HA, Aldosariand SM, Tounsi A. Study on stability and free vibration behavior of porous FGM beams. Steel Compos Struct, An Int J 2022; 45(1): 67-82

[72] Kehli A, Nebab M, Bennai R, Atmane HA,Dahmane M. Dynamic characteristics analysis of functionally graded cracked beams resting on viscoelastic medium using a new quasi-3D HSDT. Mech of Adv Mater Struct 2024; 31(30): 12651-12664.

[73] Hadji L, Atmane HA, Tounsi A, Mechab I,Adda Bedia EA. Free vibration of functionally graded sandwich plates using four-variable refined plate theory. Appl Maths Mech 2011; 32: 925-942.

[74] Zouatnia, N, Hadji L. Static and free vibration behavior of functionally graded sandwich plates using a simple higher order shear deformation theory. Adv mater Research 2019; 8(4): 313-335.

[75] Sahan MF. Transient analysis of cross-ply laminated shells using FSDT: Alternative Formulation. Steel Compos Struct 2024; 18(4): 889-907.

[76] Temel B, Noori AR. A unified solution for the vibration analysis of two-directional functionally graded axisymmetric Mindlin–Reissner plates with variable thickness. Int J Mech Sci 2020; 174(3):105471

[77] Ziari S, Belakroum R, Hammadi F. Finite element model to investigate free vibration and aeroelastic instability of functionally graded rectangular plates. Mech Adv

Mater Structs 2025; 32(7): 1391-1405.

[78] Temel B, Şahan MF.An alternative solution method for the damped response of laminated Mindlin plates. Compos Part B: Engg 2013; 47: 107-117.

[79] Dhuria M, Goyal K, Grover N. Numerical assessment of bending and buckling analysis of sigmoid functionally graded (S-FGM) porous plates in framework of secant hyperbolic shear deformation theory: A finite element study. Mech Based Des Structs Mach 2025; 1–25. https://doi.org/10.1080/15397734.2025.2473025

[80] Ali MI, Azam MS. Exact solution by dynamic stiffness method for the natural vibration of porous functionally graded plate considering neutral surface. Proc Inst Mech Engg, Part L: J Mater: Des Applications 2021; 235(7): 1585-1603.

[81] Ali MI, Azam MS. Dynamic stiffness formulation for out-of-plane natural vibration of elastically supported functionally graded plates. Int J of Struct Stab Dyn 2021; 21(05):21500621-31.

[82] Matsunaga H. Free vibration and stability of functionally graded plates according to a 2-D higher-order deformation theory. Compos Struct 2008;82(4): 499-512.

[83] Vel SS, Batra RC. Three-dimensional exact solution for the vibration of functionally graded rectangular plates. J Sound Vib 2004; 272(3-5):703-730.

[84] Pradyumna S, Bandyopadhyay JN. Free vibration analysis of functionally graded curved panels using a higher-order finite element formulation. J Sound Vib 2008; 318 (1 2):176- 192.